

Kinetics of Chronic Human Viruses -  
Comparative Analysis of Bio-Mathematical  
Models and their Clinical Implications

Jessica Rose

The Mina and Everard Goodman Faculty of Life Sciences, Bar Ilan  
University

Ph.D. Thesis

Submitted to the Senate of Bar-Ilan University

Ramat Gan, Israel

Feb 2013

## **Chapter 1**

### **1 Introduction**

Viral dynamics modeling has been invaluable in propelling our understanding of how viruses work intra-host and also in the quest to elucidate antiviral treatment and immune response mechanisms. Since clinical trials are costly and time-consuming and the immunological effects of treatment are often not clearly defined, it is prudent to explore alternative means to investigate these mechanisms. Mathematical modeling allows for an unobtrusive, safe means by which to test various theories pertaining to treatment strategies. Mathematical models are the tools we use to gain theoretical access to the real world. The generic (basic) model of HIV/HSV infection [31, 65, 66] has been used extensively by biologists and mathematicians alike to study many different aspects of viral dynamics but with evolving ideas and new data sets comes the need for the development of novel models. In this work, we had access to two unique data sets testing the efficacy, safety and bioavailability of two different antiviral drugs aimed specifically against HSV and CMV. We use mathematical modeling to explore novel concepts and theories in both cases and have gained potentially vital knowledge applicable in the clinical setting through their use.

#### **1.1 HSV**

Although a vaccine against HSV has been successfully introduced in developed countries, HSV remains a worldwide health threat. More than 400 million people living in developing countries are chronically-infected. There are over 600,000 deaths per year in the USA and Europe due to HSV and every year,

there are 100,000 new infections [63, 95]. In Israel, the estimated prevalence of HBV chronically-infected individuals is 2%, with a large variation of HBV genotypes [95, 97]. Chronic HBV results in liver failure and cancer in a large fraction of patients. Pathogenesis depends on the infection type and importantly, on HBeAg status [8, 27, 29, 32, 45, 49, 51, 57, 58].

HBV has a complex life cycle that involves the interaction of a number of replication pathways. The viral genome is circular partially double-stranded DNA that is transformed to covalently closed circular (cccDNA) which is used for synthesis of viral RNA that in turn, is reverse-transcribed to genomic DNA via viral polymerases. The viral DNA also gets integrated into the cellular DNA in a fraction of infected cells [27, 29, 40, 45, 54].

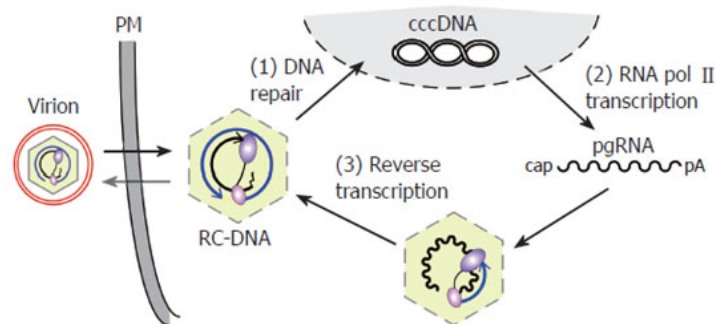


Figure 1: HBV replication cycle and the role and preservation of nuclear, episomal cccDNA.<sup>1</sup>

<sup>1</sup> Courtesy of the Feria Journal of Medicine

It is vital that cccDNA is formed during the infection/replication process in order to ensure that the stability of the viral genome is not lost during cell division so as to subsequently ensure persistent infection. Hepatocytes are the cells in the human body that most efficiently support HBV replication. The virus gains entry to the host cell via surface receptor (envelope glycoprotein) binding and viral-cell membrane fusion. The HBV nucleocapsid translocates through the cytoplasm to the cell nucleus and the viral DNA enters the host cell nucleus. The single-stranded gap in the partially double-stranded DNA is repaired and the genomic viral DNA matures into covalently closed circular DNA (cccDNA). The cccDNA is then transcribed by host-cell RNA polymerases (Pol) and the resulting RNAs are translated in the cytoplasm. The transcript encoding the HBV Pol works as a replication intermediate, namely, as pre-genomic RNA. (HBV replicates through reverse transcription with the pre-genomic RNA.) Synthesis of the negative and positive DNA strands follows; the latter synthesized by HBV Pol [64, 77]. The particle then acquires envelope glycoproteins from the golgi and the endoplasmic reticulum and is ready for budding (Figure 1). The progeny are subsequently released via the cell membrane [27, 34, 38, 40]. During HBV infection, cccDNA accumulates in cell nuclei and persists as a stable episome and acts as a template for the transcription of viral genes.

This replication process can be divided into two main steps: pre-genomic integration and post-genomic integration. The cell is infected at both steps but in different modes. Pre-integration infection indicates that the cell is infected and carries cccDNA. Post-integration infection indicates that the cell is infected

whereby the viral DNA has integrated itself into the host-cell genome, while cccDNA continues to persist as well. HBV cccDNA is responsible for viral persistence in chronic HBV infection and during prolonged antiviral therapy<sup>2</sup>. Again, it is highly stable and is carried through in host cell division. Each cccDNA is maintained in the nucleus of infected cells at a level of 1-50 copies per cell [30, 39, 85, 86].

In addition to viral particles, a large number of non-infectious antigenic particles, in particular HBeAg and HBsAg are produced in excess during the viral life cycle either through the viral replication pathway or through host-dependent pathways from the integrated virus [27, 29, 40, 45, 57, 58, 88] (Figure 2). The HBe proteins are a proteolytic cleavage product of the core protein. They are seen in acute infection and then cleared if the HBV infection resolves. However, they are characteristic of chronic infection and high infectivity. Anti-HBe develops when virus is cleared so the appearance of anti-HBe antibodies coupled with clearance of viral DNA is usually a good sign of HBV clearance. Indeed very few patients, once they develop anti-HBe antibodies, seem to then revert to HBe antigen positivity again. Thus, these antigens (and their specific antibodies) have important roles in diagnosis and characterization of the disease and as end-points for treatment evaluation. In particular, the loss of these antigens is highly predictive of treatment success [8, 14, 16, 18, 42, 57, 58, 68, 83]. Furthermore, viral antigens play important roles with respect to immune recognition and also viral masking from the immune system. Thus,

---

<sup>2</sup>Chronic infection is defined by the presence of serum HBsAg for at least 6 months, high (>10<sup>6</sup> cp/ml) serum HBV-DNA levels and higher than normal (1.2-10×) serum ALT levels.

HBV antigens are central to a complicated network of dynamical interactions between infected cells and various immune components with important clinical implications.

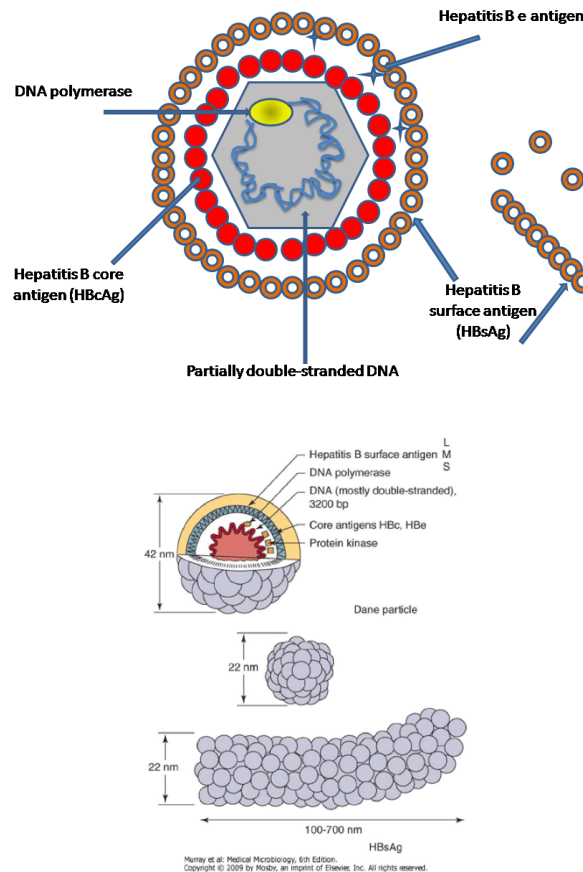


Figure 2: HBV dane particle with its component parts. The genome of HBV is made of circular DNA – not fully double-stranded<sup>3</sup>.

Generally, treatment of chronic HBV entails lifelong therapy with polymerase-inhibitors and in rare cases, shorter duration of *interferon-α* based therapy [8, 16, 17, 19, 27, 32, 43, 50, 78]. Although the anti-viral efficacy of anti-HBV

<sup>3</sup> Extracted from *Medical Microbiology*, Murray *et al.*

drugs has considerably increased over the last 10 years, the effect on HBV antigen levels is not as predictable. HBeAg loss is defined as the decline of HBeAg levels to below the limit of detection as determined by a qualitative measurement assay. Only approximately 50% of treated patients experience HBeAg loss to undergo a switch in HBeAg status from positive to negative even when the viral load drops to undetectable levels indicating that HBeAg loss is independent of the viral load decay [57, 58]. This implies a dependence on some other variable. HBeAg is not necessary for viral replication but rather is considered to be a by-product of the viral replication process and determines the infectivity of the patient [29, 54, 57, 58]. Its persistence in chronically-infected individuals could be due to a number of potential factors but we think it is linked to the number of persistent cccDNA-infected cells. Inevitably, different individuals will have different infected cell clearance rates/patterns due to differences in immune response effects, responses to treatment, and a number of other factors such as rates of production and clearance of HBeAg and HBeAb, for example.

A proportion of cells that carry cccDNA<sup>4</sup> produce HBeAg, and therefore we theorized that this easily detectable antigen could be used as a surrogate marker of the number of infected cells and could be used to help clarify the relationship between viral decay, HBeAg loss and cccDNA-infected cell loss in the context of antiviral treatment [57, 58]. During the replication process, antigens are produced in excess, as reported. The type of antigen and the quantity detected

---

<sup>4</sup>The number of cccDNA per infected cell varies from cell to cell and determines the amount of virus released by each infected cell.

can indicate the stage or level of infection or the replication status of the virus. Only when there is a great deal of viral replication does a significant amount of virus reach the blood. An HBeAg test is used to determine if a patient infected with HBV is infectious; patients with anti-HBeAg are not considered infectious. Patients who have chronic HBV hepatitis with positive HBeAg status are deemed infectious and typically have a much worse prognosis, whereas patients with chronic HBV infection and negative HBeAg status are not considered to be as infectious [29]. Recently, by using a specific real-time PCR assay, a study indicated that 48 weeks of *adefovir dipivoxil* (*adefovir*)<sup>5</sup> therapy could result in a significant 0.8 log<sub>10</sub> decrease in cccDNA copies/cell<sup>6</sup> [30, 85, 86]. However, because HBeAg is transcribed by host factors, treatment does not directly block HBeAg production [27, 29]. Biologically, adefovir acts to interfere with the process of DNA replication by blocking the enzyme reverse transcriptase<sup>7</sup> to hinder the production of new virions. Thus HBeAg presumably continues to be produced at normal rates by the cccDNA-infected cells throughout treatment. We assume that it is the decrease in the number of infected cells that eventually causes the observed decrease in HBeAg and that is not simply due to viral load decline.

Studies of HBV kinetics have helped us to understand more about how the virus operates within the human host, and how the host immune system reacts [60, 61, 68, 69, 81, 87, 90, 98, 99]. Using a simple novel model of HBV infection,

---

<sup>5</sup> An orally-administered nucleotide analog reverse transcriptase inhibitor

<sup>6</sup> Diagnosis of Hepatitis B Virus Infection: Intrahepatic HBV cccDNA Pool

<sup>7</sup> Reverse transcriptase is a DNA polymerase enzyme that transcribes single-stranded RNA into single-stranded DNA.

we examined the relationship between HBeAg loss and viral load decay in the context of varying a treatment parameter and an immune response parameter to simulate the effects of treatment and the immune response in order to elucidate the mechanisms of viral blocking and the immune response. We assume that the amount of HBeAg produced by a single infected cell remains constant in the presence of treatment.

Our goal was to use the model to show that HBeAg loss is dependent on cccDNA-infected cell loss and not solely on viral decline. Following validation of our novel model of HBV infection, we used it to provide evidence that optimal clinical prognosis is not necessarily dependent on higher dose of treatment and that an effective immune response does in fact yield earlier HBeAg negativity. This is based on the relationship between HBeAg and the number of remaining cccDNA-infected cells: if the HBeAg does not become negative, then it is possible that the number of cccDNA-infected cells remaining in the host is high, irrespective of the viral load. This would explain the pathology associated with positive HBeAg status.

It has been shown that the amount of cccDNAs (cp/cell) is positively correlated with HBeAg status. That is, when the number of copies per cell is high, HBeAg status is positive; when the number of copies is low, HBeAg status is negative [30, 85, 86]. This will not be approached from the modeling point of view since our model is a cellular model that includes the population of cccDNA-infected cells as an explicit variable and not the number of cccDNAs/cell. Future work would involve the development of an intracellular model to address this.

## 1.2 CMV

CMV or cytomegalovirus (from the Greek *cyto*=cell; *megalo*=large)<sup>8</sup> got its name from the effect of infection of cells which is enlargement. CMV is a common herpes virus (Human Herpesvirus-5) that infects most people at some point in their lifetime and is generally asymptomatic. When it does cause symptoms, they often resemble those of Infectious Mononucleosis. Approximately 50% to 80% of adult individuals in the United States are infected based on seropositivity [95]. There is no vaccine against CMV. CMV is generally associated with salivary glands and can be transmitted by exchange of saliva and other bodily fluids. Figure 3 shows a CMV virion with its membrane glycoproteins and its nucleocapsid holding the genetic material which comprises double-stranded DNA of more than 240 kbp (Figure 3). Cytomegalovirus gets its name from its very large size, microbiologically-speaking.

Upon infection, most infected cells are cleared via CMV-specific CD8<sup>+</sup> T cells and the virus becomes latent for the duration of the infected individual's life. Therefore, CMV is generally an innocuous virus. However, in an immunocompromised setting such as a transplantation setting, CMV can become problematic and cause serious pathologies. The reason for this is that life-long immunosuppression is the standard of care for transplantees and therefore, the immune system, which normally suppresses CMV, is disabled. Therefore, CMV can become reactivated or a primary infection can ensue. Over half of all

---

<sup>8</sup> Wikipedia - Cytomegalovirus

transplantees become chronically CMV-infected [3, 4, 6, 10, 11, 15, 25, 26, 67, 74, 76].

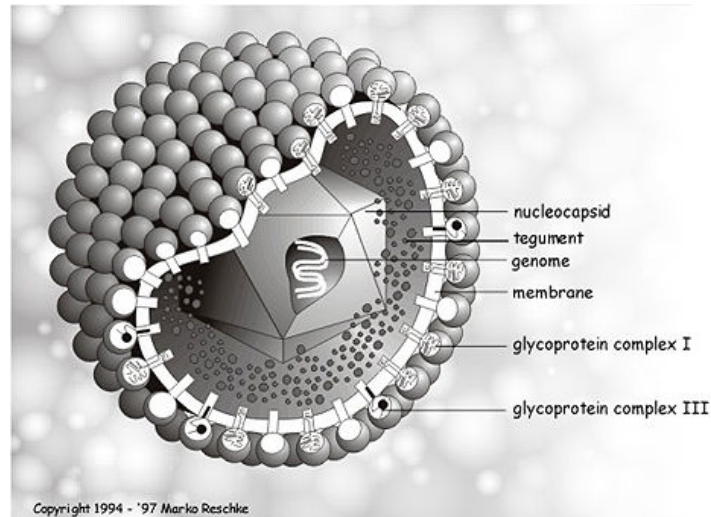


Figure 3: CMV virion with its component parts: courtesy of Marko Reschke and Markus Eickmann, Institut für Virologie, Marburg, Germany [75].

Depending on the type of organ or cells transplanted and the CMV status of the donor and recipient and the treatment protocol, CMV may become reactivated or a primary infection may ensue at different times ranging from 10 days to months [3, 11, 27].

There are four possible donor (D) and recipient (R) combinations based on whether or not D and/or R are CMV seropositive:  $D^+/R^-$ ,  $D^-/R^+$ ,  $D^+/R^+$  and  $D^-/R^-$ , the latter being a control group. The worst combination is  $D^+/R^-$  and accounts for approximately 20% of all solid organ donor transplants. This is because a CMV-naïve recipient is susceptible to primary infection due to the presence of virus in the donor organ. The more favorable combinations are  $D^-/R^-$  or  $D^-/R^+$  because an organ from a CMV-negative donor poses the least threat

regardless of the donor status. Nevertheless, dormant virus in the recipient can become activated even if the donor organ is negative. Thus, CMV can pose a significant threat to both patient and graft health. Antiviral drugs are generally prescribed either preemptively or prophylactically in order to cope with CMV in the transplantation setting. However, it is unclear which drug or treatment protocol is optimal. The most effective prophylactic antiviral drug in clinical trials now is *IV* GCV or its oral pro-drug *Valganciclovir* (VGCV): both are aimed specifically against CMV. Another drug Artesunate (ART) which is actually an antimalarial drug has also shown promise to reduce CMV viral loads and is a desirable choice due to low toxicity and side-effects.

The CMV replication cycle is complex and comprises three distinct phases: productive infection, latent infection and reactivation [13, 27, 34]. Productive infection is characterized by the synthesis of new infectious virus, resulting in death of the host cell. Latent infection follows productive/primary infection where CMV can enter a dormant state characteristic of all herpes viruses during which time infectious virus is not produced [27]. The latent phase of infection lasts for the life of the host and in a healthy immune system keeps viral resurgence at bay. It is not entirely clear what underlies the mechanism of latency. Reactivation involves a reversion from the latent state to a chronic productive infection state whereby virus reemerges in the blood and other mucous-membrane-associated areas. CMV reactivation does not necessarily lead to chronic infection; it is just the reversion from latent into productive/lytic infection which, in most cases, lasts only a few days.

Figure 4 shows the intracellular activity of CMV as it enters a host cell, and in particular, where and how GCV acts to interfere with the replication process. This is the productive infection step whereby treatment (GCV) interferes with elongation of linear DNA which is used as a template for the production of new virions. The virus gains entry to the host cell via cell surface receptors and dumps its contents into the cytoplasm of the cell.

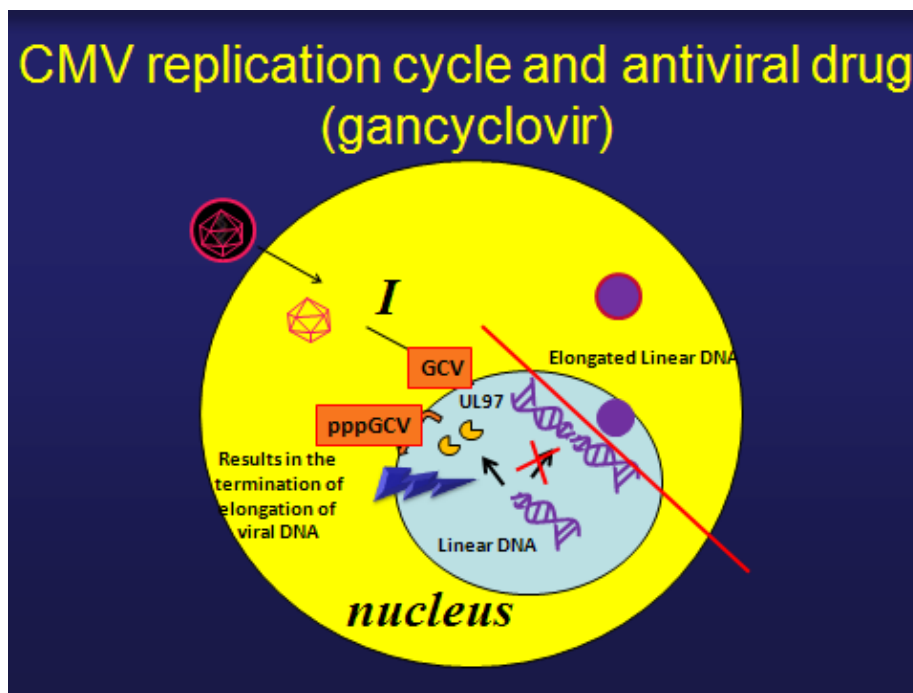


Figure 4: CMV replication cycle

The component parts move to the nucleus where the linear form of the viral DNA gets extended to form long linear DNA strands. These are cleaved for eventual use in the formation of new virions. CMV replication starts with the transcription of the immediate early (IE) genes driven by cell RNA polymerase II guided by viral transcription factors. Some of the IE genes then act on the early promoters to drive cell RNA pol II transcription of these genes (many including DNA pol being involved in genome replication). Amplification of

viral DNA is followed by rolling circle replication which produces concatemers that will ultimately be cleaved and packaged into new virions [24, 27]. The transcriptional profile of the amplified genome DNA is not well characterized but the virus needs to produce late mRNAs to produce the proteins for DNA packaging. During the process of replication (early gene), viral proteins are produced in excess. One of these proteins is an enzyme called UL97.

A unique property of GCV is its mode of action in the host. It relies on the viral enzyme UL97 to become metabolized to impose its antiviral properties. Figure 5 shows schematically how this interaction takes place.

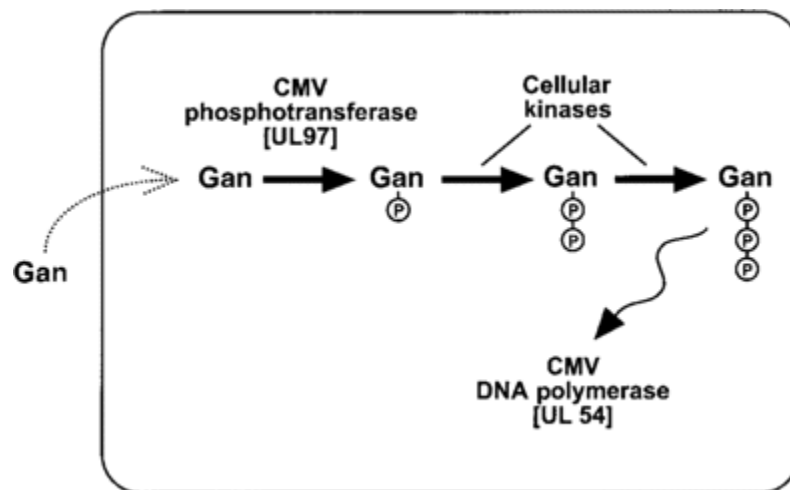


Figure 5: The dependence of GCV on UL97. To be active, GCV must be converted to a tri-phosphorylated form; this conversion occurs via 3 sequential phosphorylation steps, the first of which is performed by a virally encoded phosphotransferase (product of UL97). The 2 subsequent phosphorylation steps are performed by cellular enzymes, and the tri-phosphorylated form of

GCV ultimately preferentially inhibits CMV DNA polymerase (product of UL54).<sup>9</sup>

*Artesunate* (ART) is an antimalarial agent that is primarily used as part of a multi-drug treatment regimen to treat malaria. It is an artemisinin derivative and is safe and well-tolerated<sup>10</sup>. Recently, it has also been shown to be effective at treating CMV [73]. ART is not nephrotoxic and is believed to inhibit viral replication via an alternate mechanism of action to DNA polymerase and exhibits no cytotoxicity [75]. This makes it an attractive choice for treating CMV since GCV and other anti-CMV drugs are highly toxic.

### **1.3 Bio-Mathematical Modeling**

Mathematical modeling is a very useful tool for analyzing how a system evolves in time and how it reacts to perturbations such as initiation of treatment. Mathematical models in general, are sets of equations that describe the behavior of a system via dependent and independent variables.

*Kinetic analysis* is the investigation of measurements (of model variables) sampled over time. It allows both qualitative and quantitative characterization of the time-dependent progress of each (model) variable [7, 20]. Generally, these processes are observed and studied using time-series plots. Qualitatively, patterns of kinetic trends, and changes in these trends, can be obtained. Quantitatively, growth and decline rates and their magnitudes can be estimated

---

<sup>9</sup> Ajit P. Limaye, Ganciclovir-Resistant Cytomegalovirus in Organ Transplant Recipients, *Clin Infect Dis.* (2002) 35 (7): 866-872.

<sup>10</sup> WHO (2006) *Guidelines for the treatment of malaria.* pp251.

from the slopes of variable trajectories generated by a kinetic profile. We can also use kinetic analysis to observe potential qualitative and/or quantitative changes that may occur as a result of perturbing the system such as is the case when treatment potency is varied. For example, if a parameter representative of treatment is introduced to a mathematical model, we can examine potential changes in both qualitative and quantitative behaviors of the system as this parameter is changed. This is synonymous to different dosing in a clinical setting. Likewise for a parameter representative of immune function which would be synonymous to different immune states or functionalities, or due to immune enhancement treatment, for example. We can subsequently make predictions pertaining to viral load resurgence, for example, without having to endanger patients. The value in this strategy is multi-fold and has proven very useful over the years.

Viral pathogenesis is associated with changes in the sizes of both cellular and viral populations as the immune system attempts to eliminate the virus from the host. The state of the 'infected' immune system at any time  $t$  is specified by the values of the variables at time  $t$ . Many mathematical models that describe these systems involve nonlinear differential equations because the variables in the model usually do not change in direct proportion to other variables. In general, exact solutions cannot be found for nonlinear systems. Therefore, analysis of such nonlinear dynamical systems is commonly approached in a qualitative manner, especially when the system involves many variables. This is because the components of the equations that make up the system are not known precisely. *Dynamical systems analysis* allows us to find the eventual behavior

of a system without having to know parameter values accurately or even having to know the terms of the system precisely. By analyzing the system in a qualitative manner, we do not have to rely on numerical techniques which, in turn, rely on the validity or precision of the equations from which they originate. This is especially useful in complex model analysis and for models with many variables [7, 20, 66].

#### 1.4 Modeling HBV

As with any modeling pursuit, the first step is to check if we can describe what we see in data using the simplest model that we can. Perhaps the most well-known dynamical system used to characterize HBV infection, also known as the basic model of infection, is that of Alan Perelson and colleagues [31, 65, 66]. This basic model was originally designed to study HIV infection and describes the rate of change of three variables: uninfected target cells,  $T$ , infected target cells,  $I$ , and virus particles,  $V$ , at any time  $t$ . The model is a system of three ordinary differential equations (ODEs). The equations for this basic model are as follows.

$$\begin{aligned}\frac{dT}{dt} &= s + pT\left(1 - \frac{T}{T_{\max}}\right) - dT - kVT \\ \frac{dI}{dt} &= kVT - \delta I \\ \frac{dV}{dt} &= N\delta I - cV\end{aligned}$$

The parameters are  $s$ ,  $p$ ,  $T_{\max}$ ,  $d$ ,  $k$ ,  $\delta$ ,  $N$  and  $c$  and represent rate constants. Uninfected target cells enter the system from the thymus at a constant rate  $s$ . The growth of this population is assumed to be logistic in that it can only grow until it reaches a carrying capacity  $T_{\max}$ . This carrying capacity is regulated by

homeostatic mechanisms that regulate overall T cell numbers: there are a finite number of cells that can occupy the body at any given time.  $p$  is the intrinsic growth rate. Target cells will ultimately die at some constant rate also as part of normal homeostatic mechanisms.

When the virus enters the system, the susceptible uninfected target cell population becomes infected at rate  $k$  (proportional to  $T$  and  $V$ ). This creates the population of infected target cells,  $I$ , whose members die at a constant rate  $\delta$ . As each infected cell dies a certain number of virions ( $N$ ) are released into the body. The virus also dies by natural processes at a constant rate  $c$ . The model predicts a single stable fixed point  $(T; I; V)$  with positive fixed-point coordinates. These coordinates vary according to the parameter values selected. This basic model has allowed crucial insights into the ‘fast’ dynamics of the virus and how it reacts to antiretroviral treatment. Antiretroviral treatment is introduced to the equations as a parameter that modifies the infection rate  $k$  or the production rate of virus  $N$ . The viral turnover rate is extremely high; higher than previously estimated or assumed [31, 65].

Numerous other models utilize the fundamental concepts of this basic model as it quite elegantly and simplistically describes the general behaviours of the variables  $T$ ,  $I$  and  $V$  and how they change together in time both in the presence and absence of treatment. Of these, include models that have contributed to our understanding of the effector T cell role in HBV infection and advanced our understanding of immunopathogenetic factors such as the models developed by Martin Nowak, Charles Bangham and Sebastian Bonhoeffer and colleagues [61,

62]. Collectively, they extended the basic model of viral infection to include a CTL population to account for the effects of virus-specific cells that kill infected cells [61]. John Murray and colleagues built a multi-dimensional model to explore T cell effector functions in the context of hepatitis B virus (HBV) infection in chimpanzees [53]. In addition, Piero Colombatto and colleagues developed a new model that described the dynamics of HBV-DNA and infected cells in the context of antiviral treatment aimed specifically against HBV [16, 17]. Avidan Neumann and colleagues used mathematical modeling as tools to make predictions pertaining to viral and HBeAg decay kinetics in order to further our understanding of the relationships between particular antivirals, the virus and its antigens [42, 57]. Studies of the particular phases of HBV infection, acute and chronic, have also been done using mathematical modeling such as the work by Alan Perelson and colleagues on the kinetics of acute HBV infection [86] and the work by L.M. Wolthers and colleagues investigating viral dynamics in chronic HBV infection [90, 91, 92].

We also use the basic model as the basis of our novel model of HBV infection. Our model includes all the variables of the basic model of infection but with an additional variable to represent the HBeAg population. We will describe the model and its development and use in Chapter 3.

## **1.5 Modeling CMV**

We tested the basic model of infection to see if it was sufficient for our needs in this work: that is, whether or not it was able to yield the unique kinetic profile

patterns seen in data. It was not. Thus, we developed a new model of CMV infection that could not only yield the unique kinetic profiles but that also included the feedback loop between GCV and UL97.

Of the existing models of CMV infection is the model developed by Grace Kepler that describes the primary, latent and reactivated infections in immunocompetent or immunocompromised individuals [36, 37]. This model is a five-dimensional system of ordinary differential equations and exhibits primary, latent, and secondary (reactivated) infections whereby latent infection is characterized by low-level viral load and actively-infected cells. We ran simulations using this particular model and could not yield all of the kinetic profiles from our data. Thus, as descriptive of the biological interactions as this model may be, it was not useful to us.

Another leader in CMV modeling is Vincent Emery who recently published findings pertaining to the VICTOR<sup>11</sup> data using the basic model of infection [24, 25, 26]. Emery was also instrumental in the development of the biological concepts that underlie our novel model. Again, since our goal was to elucidate unique kinetic profile patterns seen in data and not to simply estimate replication rates for example, we needed to think outside of the existing boxes. Thus, we used the basic model of infection as a template and built an intracellular model of infection that includes new variables to account for the intracellular feedback loop between the drug and UL97. Our new model appropriately describes all

---

<sup>11</sup> VICTOR Study - A Study of Valcyte (Valganciclovir po) Compared to Ganciclovir iv in Patients With Cytomegalovirus (CMV) Disease Who Are Solid Organ Transplant Recipients  
19

observed kinetic profile patterns. Since the model is a system of ordinary differential equations, we analyze it in much the same way as a cellular model of infection.

In the process of developing the model in this thesis, we first developed and tested a number of different prototype models ranging from four to eight-dimensional systems of ODEs. We tried to capture the dynamics to explain the kinetic patterns by incorporating the concepts of pharmacokinetic changes, different cellular compartments and different physiological compartments, changes in immune response and evolution of resistance. However, none of these models accurately captured the observed viral kinetics and the accompanying observations from the VICTOR clinical study. It wasn't until we introduced a model with intracellular variables which describe the interaction between GCV, UL97 and CMV that we were able to explain all of the observations from data.

## **1.6 Thesis Structure**

This thesis is subdivided into three parts as my work involved three separate projects. The first chapter focuses on viral kinetic studies of HBV and the relationship between HBeAg and HBV-DNA kinetics. The second chapter explains the effects of the intracellular feedback loop between CMV and GCV on CMV kinetics. The third chapter is an analysis of the effects of the antimalarial drug artesunate which again, has been shown to be effective against CMV to reduce CMV viral loads. In all three studies, we made unique and interesting observations using mathematical modeling as a tool and were able

to make predictions and answer questions pertaining to each respective study to advance our understanding of viral kinetics, mechanisms of treatment and the effects of the immune response. More importantly, these results may have clinical implications in the context of dose, on-treatment immune enhancement and multi-drug therapy.

## **Chapter 2**

### **Methods**

Mathematical simulations and calculations of fixed points and eigenvalue problems were done using *Madonna Berkeley* software and *Maple* software, respectively. Parameter estimates were derived from the literature and unknown parameter values were either estimated or calculated. Since data integration is an integral part of this project, we also employed *Excel v.2007* and *SPSS v.15* software to perform statistical analyses to examine potential correlations, associations and relationships between variables. In the HBV work, differences in viral loads and times to HBeAg loss between patient groups were examined using the Fisher exact test or the Wilcoxon signed-rank test. The statistical significances of differences in the viral loads when HBeAg became negative ( $V_{Neg}$ ) and the time at which this occurred ( $t_{Neg}$ ) between patient groups (according to antibody status) were tested using the nonparametric Mann-Whitney U-test. For further quantitative comparison of HBeAg levels, we used statistics from a recent study on the effects of pegylated interferon alfa-2a on early on-treatment characteristics in patients with chronic hepatitis B infection [78]. The baseline HBeAg load was measured using the Paul Ehrlich Institute Unit per milliliter (PEIU/ml).<sup>12</sup>

## 2.1 Steady state or fixed point solutions

Fixed points are locations in phase space. Phase space is the set of all possible states of a system. The dimension of the phase space is the number of variables in the system. The path in phase space traced out by a solution of a system is called an orbit. A fixed point is a special type of orbit that is just a single point

---

<sup>12</sup> The Paul Ehrlich standards are calibrated in ng/ml and therefore relate to highest metrological level.

in phase space as the system changes with time. A fixed point, also known as an equilibrium or steady state, corresponds to a motionless state of a system and can be stable or unstable. A fixed point is (asymptotically) stable when it attracts all nearby orbits in phase space. A fixed point that is unstable repels nearby orbits in phase space. Every fixed point inherently has a stability property [7, 20].

Since our novel models are four and six-dimensional systems of ordinary differential equations, we chose to solve the models both by hand and with the help of *Maple* software (due to the complexity of the solutions in the higher dimensional model), respectively, to find the fixed points and their stabilities. The analysis of the models was done by running time series simulations using *Madonna Berkeley* software to map and predict the behaviour of the time series trajectories and these were compared quantitatively and qualitatively with kinetic patterns from data. In order to run time-series simulations for the models, we simply require the steady state solutions as initial conditions to provide a starting point for the simulations. We do this because in most cases we do not have sufficient pre-treatment viral kinetic information and thus it is difficult for us to determine the dynamics pre-therapy. Hence, for simplicity, we use the steady-state approximation. If therapy started at CMV primary infection or during an oscillation in HBV, we would not need to use this method.

## **2.2 Analytical expression relating viral load to HBeAg level**

As part of the modeling process, we calculated an expression to describe the relationship between the viral load and HBeAg level. If we assume a quasi-steady state and make a second assumption that for  $E < E_x$ ,  $E$  is undetectable, then since  $E=f(I)$  then  $E=f(I) < E_x$ . Furthermore, since  $I=g(V)$  and thus  $f(g(V)) < E_x$ . Therefore,  $V < h(E_x)$  where  $h(E_x)$  is a function of some or all of the parameters. This necessitates the assumptions that the functions are reversible and monotonic.

We call the virus load when HBeAg is lost  $V_{\text{Neg}}$ . We assume that HBeAg loss is due to the presence of treatment and its indirect effect on the number of infected cells. The burst size of the virus is defined by the expression  $(1-\epsilon)p_v/c_v$  (where  $p_v$  is the growth rate and  $c_v$  is the death rate of the virus) and the burst size of the HBeAg is defined by the expression  $p_e/c_e$  (where  $p_e$  is the growth rate and  $c_e$  is the death rate of HBeAg). Therefore, the ratio of the burst size of the virus to the burst size of the HBeAg can be written  $(1-\epsilon)p_{vc_e}/c_v p_e$ . For the chosen parameter values,  $(1-\epsilon)p_{vc_e}/c_v p_e = 1000$ .

The levels of  $I_{c0}$ ,  $E_0$  and  $V_0$  at quasi-steady state are related by setting  $dI_c/dt=0$ ,  $dE/dt=0$  and  $dV/dt=0$ , ( $\epsilon=0$ ).  $T_0$  is the baseline target cell level which is assumed to remain relatively constant. When we solve, we get  $V=(1-\epsilon)p_v I/c_v$  and  $E=p_e I/c_e$ . Therefore,  $V/E=(1-\epsilon)p_v I/c_v / p_e I/c_e$  which is exactly the expression  $(1-\epsilon)p_{vc_e}/c_v p_e$ . We can easily write the condition for which  $V_{\text{Neg}} < h(E_x, \text{parameters})$  as  $V/E \cdot E_x = (1-\epsilon) p_{vc_e}/c_v p_e \cdot E_x$ .

Generally,  $V_{\text{Eneg}} < \text{burst size } V / \text{burst size } E = (1-\varepsilon)p_{\text{vcE}}/c_{\text{vpE}} \cdot E_x$ . This expression predicts the viral load at the time of HBeAg loss. We can therefore predict  $V_{\text{Eneg}}$  for any parameter set. Notice that when treatment is introduced, we have  $V_{\text{Eneg}} < (1-\varepsilon)p_{\text{vcE}}/c_{\text{vpE}} \cdot E_x$ .

### 2.3 Reproductive ratio for HBV modeling

Before infection,  $I=0$ ,  $E=0$  and  $V=0$ , and uninfected cells are at equilibrium  $T=s/d$ . When infection occurs the initial conditions at the start of infection are  $T_0=s/d$ ,  $I_0=0$ ,  $E_0=0$  and  $V_0$ . Whether or not the virus grows to establish an infection depends on the reproductive ratio,  $R_0$ . The rate at which one infected cell gives rise to new infected cells is given by the expression  $\beta p_V T / c_V$ . Since the lifetime of an infected cell is  $1/\delta$ , we obtain  $R_0 = s \beta p_V / d \delta c_V$ . If  $R_0 < 1$ , then every infected cell will produce less than one other infected cell meaning that the virus will die out. If however,  $R_0 > 1$ , then every infected cell will produce at least one newly infected cell meaning that the virus can establish an infection.

When treatment is incorporated we have  $(1-\varepsilon)R_0 < 1$ . If  $\varepsilon > 1 - 1/R_0$ , then the virus will be eradicated. Thus, the conditions for eradication of the virus are such that  $\varepsilon$  is larger than some value which is based on the reproductive ratio. For example, if  $R_0=10$ , then in order for the virus to be eradicated,  $\varepsilon$  must be greater than 90%. Thus, if  $\varepsilon > \varepsilon_{\text{crit}}$  (critical value for eradication of virus), then the virus is eradicated. If  $\varepsilon < \varepsilon_{\text{crit}}$ , then the virus persists at low levels. If however,  $\varepsilon = \varepsilon_{\text{crit}}$ , then we know that the virus population is in equilibrium with treatment.

We equate efficacy of treatment to the rate at which the viral load declines in the first few days (1<sup>st</sup> slope/phase). In the HBV model, the treatment parameter

acts to reduce the production rate of virus whereas in the CMV model, the treatment parameter acts to reduce the production of linear (short) DNA. Similarly, in the case of the HBV model, we equate the efficacy of the immune response to the rate at which infected cell loss occurs thereafter (2<sup>nd</sup> slope/phase). It must be noted here that the immune response responsible for infected cell loss is antibody *inclusive* but not *exclusive*. Therefore for the sake of simplicity when we compare the data to the model, we can loosely equate the potency of  $m$ , the immune response parameter, to antibody status. That is, if antibody status was positive, then we can assume that the value of  $m$  is higher than it would be if the antibody status was negative.

### **Chapter 3**

## **Kinetic modeling of Hepatitis B Virus: the relationship between HBeAg and viral kinetics<sup>13</sup>**

### **3.1 Introduction**

Approximately 350-400 million people suffer from chronic HBV infection. Liver diseases caused by chronic infection kill approximately 1 million people per year. HBV therefore remains at the forefront of human virus research. Studies of HBV kinetics have helped us to understand more about how the virus operates within the human host, and how the host immune system reacts. HBV covalently closed circular DNA (cccDNA) is responsible for viral persistence in chronic HBV infection and during prolonged antiviral therapy. As previously mentioned, cells that carry cccDNA<sup>14</sup> produce HBeAg through a process not affected by current anti-viral therapy, and therefore we suggest that this easily detectable antigen can be used as a surrogate marker of cccDNA infected cells to help clarify the relationship between viral decay and HBeAg status.

### **3.2 Patients and study design**

We used data from a clinical trial testing *adefovir* (ADV).<sup>15</sup> The study group was part of a Phase III clinical trial evaluating the safety and efficacy of ADV once daily (10 mg or 30 mg) as monotherapy compared to placebo in 515 HBeAg-positive patients with chronic HBV infection and compensated liver function. Of this total number of patients, 167, 171 and 173 patients had

---

<sup>13</sup> Chapter 3 is a modified extract of a paper soon to be submitted for publication and is an investigation of the relationship of HBeAg status and HBV viral kinetics.

<sup>14</sup>The number of cccDNA per infected cell varies from cell to cell and determines the amount of virus released by each infected cell.

<sup>15</sup> Study number GS-98-437, sponsored by Gilead Sciences, Foster City, CA

analyzable data in the PLB, ADV 10 and 30, respectively, where 11%, 24% and 27% experienced HBeAg loss within the first year [49]. Four patients were not included due to the fact that they took no study medication. Additional patients underwent HBeAg loss following week 48. The study participants were of genotypes A, B, C, D, E and F. We include only Genotypes A-D in our analysis due to sparse data in genotypes E and F. We selected patients whose HBeAg status was known pre and post treatment in order to make comparisons between the groups according to HBeAg and HBeAb status. Since HBeAg status was either positive or negative rather than having a quantitatively measured value, we assigned the patients a value of either 0 or 1 to correspond to being HBeAg negative or positive at the time of and during the course of treatment. Also, measurements of HBe antibody (HBeAb) were taken throughout the course of treatment (again either positive (AB0) or negative (AB1)) and we utilized this information as well for comparisons between groups. The presence of HBeAb generally indicates a favorable prognosis. As previously mentioned, not all patients experienced HBeAg loss within the first year of treatment, but we include  $V_{Neg}$  and  $t_{Neg}$  data from all patients who experienced HBeAg loss in our analysis.

### **3.3 Results**

#### **3.3.1 The data**

In order to draw comparisons between the data and the model, we examined potential differences in the median  $V_{Neg}$  and  $t_{Neg}$  in the study group in the contexts of PLB and ADV. Figure 6 is a boxplot showing a comparison between PLB and ADV (ADV 10/30) of the median  $V_{Neg}$  and  $t_{Neg}$  for all patients according to antibody status at the time that HBeAg became negative ( $t_{Neg}$ ). Group 0 (AB0) includes all patients who were Ab<sup>+</sup> at  $t_{Neg}$  and Group 1 (AB1) includes all those patients who were Ab<sup>-</sup> at  $t_{Neg}$ .

$V_{Neg}$  and  $t_{Neg}$  measurements were compared for all patients who experienced HBeAg loss. 16%, 30% and 34% of patients in the PLB, ADV 10 and ADV 30 arms experienced HBeAg loss. When we separated according to HBeAb status, we found that 5%, 13% and 12% (PLB, ADV10, ADV30, respectively) of patients in the AB0 group and 11%, 18% and 22% (PLB, ADV10, ADV30, respectively) in the AB1 group experienced HBeAg loss.

In the case of the PLB arm,  $V_{Neg}$  appears to be independent of Ab status. That is, the presence of antibodies does not appear to influence the viral load when the HBeAg is/becomes negative. In both cases (HBeAb<sup>+/-</sup>) we see the loss of HBeAg but HBeAb status appears to have no significant effect on the viral load.

In the case of the ADV arms, we observed slightly higher viral loads in Group 0 for both doses. These differences were not significant however. (ADV 10 mg patients p=0.212; ADV 30 mg patients p=0.089; Mann-Whitney test).

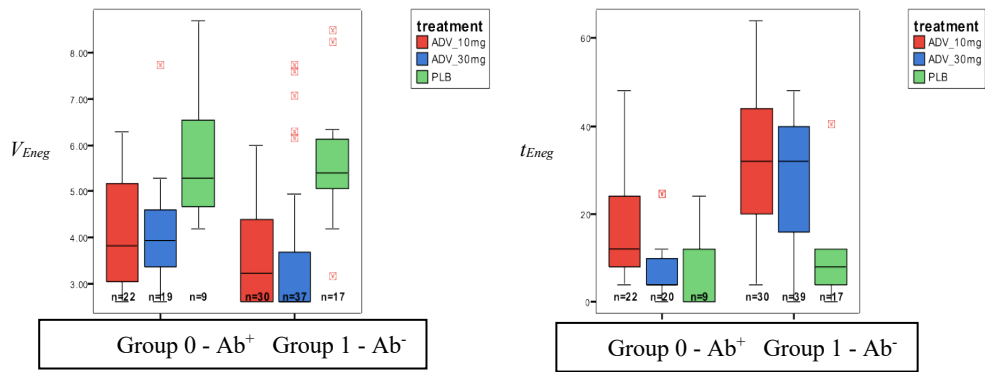


Figure 6: Comparison of the viral loads  $V_{E_{neg}}$  (left) and the times  $t_{E_{neg}}$  (right) when HBeAg became negative in the context of PLB and ADV 10 and ADV 30. The samples on the left of each boxplot represent the AB0 patients and on the right, the AB1 patients.

When we compared the PLB and ADV arms as per group (AB0 vs. AB1), we saw that the median  $V_{E_{neg}}$ s were higher in the PLB arm than in the ADV (combined 10 and 30 mg) arm ( $p=0.009$ ) and ( $p=0.001$ ). Thus, treatment is not required to induce HBeAg negativity but does in fact have a significant effect on the viral load when the HBeAg becomes negative which is independent of antibody status. This means that HBeAg negativity does not depend on viral load. It is thus plausible that HBeAg negativity is linked to infected cell loss rate and/or the number of HBeAg-producing infected cells. We will examine this further in the modeling section.

When we examined the effects of Ab status on  $t_{E_{neg}}$ , we see that Ab status does not influence  $t_{E_{neg}}$  in the PLB arm ( $p=0.887$ ). However, we see a big influence of Ab status on  $t_{E_{neg}}$  in the ADV arm.  $t_{E_{neg}}$  is shorter in Group 0 than for Group 1 (ADV 10mg,  $p=0.002$ ; ADV 30 mg,  $p=0.001$ ). This means that the time it

takes for the HBeAg to become negative is delayed when antibodies are absent. This, in turn, implies that antibodies (the humoral immune response) are playing a role in expediting the time to HBeAg loss. Bear in mind that the presence of antibodies is a signifier that the cellular arm of the immune response is activated as well and it has been shown that T-cell proliferative responses can be enhanced by treatment to induce HBeAg loss. The issue of functionality of T-cell responses will not be addressed further here. Also of note is the fact that we do not know the levels of HBeAg or HBeAb, just whether or not they are present above a certain threshold. Therefore, it could be that some patients simply have less HBeAb in relation to HBeAg. This could be a function of immune complexing. There is no significant difference between  $t_{Neg}$  according to the ADV dosage.

Thus, in the absence of treatment (PLB),  $V_{Neg}$  is higher (mean  $\sim 5.3$  log) and not influenced by the presence of antibodies; this is in comparison with ADV (10 or 30 mg). This implies that if the initial number of HBeAg-producing cccDNA-infected cells is high, that is, if HBeAg levels are high, then regardless of antibody status, the viral load at the time of HBeAg negativity will be higher. This is assuming that in the absence of treatment the number of infected cells is higher. Remember, this is in comparison with the percentage of PLB patients who actually experienced HBeAg loss which is higher for HBeAb<sup>-</sup>.

Interestingly, although not statistically significant, the viral load at the time of HBeAg loss is higher in the case where antibodies are present for both doses of ADV. It is possible that a higher level of HBeAg (albeit negative) may invoke

a higher level of HBe-antibodies. Since we do not have actual measurements for the level of HBeAg, we cannot confirm this theory clinically at this point. This should be addressed in future studies.

In the case of  $t_{Neg}$ , in the context of PLB, HBeAg becomes negative very early (within a few days) and there is no significant difference in  $t_{Neg}$  between Groups 0 and 1 ( $p=0.06$ ). In addition, HBeAg becomes negative earlier than for the ADV arms for both Groups 0 and 1. This is possibly due to the fact that the HBeAg levels were already low at the time of placebo administration. Also, in the absence of antibodies,  $t_{Neg}$  is significantly earlier than in the ADV arms. We theorize that this happens because the HBeAg level was already low. More potent treatment induces a slight delay in  $t_{Neg}$  in Group 0 and also,  $t_{Neg}$  is significantly higher for both ADV 10 and 30 in Group 1, that is, in the absence of antibodies. Thus, the presence of antibodies has a strong effect on when HBeAg loss occurs in the context of treatment.

We also examined potential differences in the median  $V_{NegS}$  in the study group for PLB and ADV in the context of genotype. Figure 7 shows a comparison between PLB and ADV (ADV 10/30) on the median  $V_{NegS}$  for four genotypes (A, B, C and D) according to antibody status at the time that HBeAg became negative. Again, group 0 includes all patients who were  $Ab^+$  at that time and group 1 includes all those patients who were  $Ab^-$  at that time. In comparing the PLB and ADV arms *without* separating by genotype, we observed that the median  $V_{NegS}$  higher in the PLB arm than in the ADV arm ( $p=0.009$ ) and ( $p=0.001$ ). When we separated the groups by genotype and antibody status, we

saw this influence in more detail. In Group 0 in the PLB arm, we see a difference in  $V_{Neg}$  among genotypes B and C whereby  $V_{Neg}$  is approximately 1 log higher in genotype B. Both are  $Ab^+$ . Also, we see this difference, albeit, slightly smaller, within the A and C genotypes in the  $Ab^-$  case. Despite these observations, the only real comparison we can make with respect to the effect of antibody status, due to sparse data, is for Genotype C. It is clear that there is no significant difference in the median  $V_{Neg}$  for this genotype related to antibody status ( $p=0.756$ ). Thus, when we separate by genotype,  $V_{Neg}$  appears to be independent of genotype and Ab status.

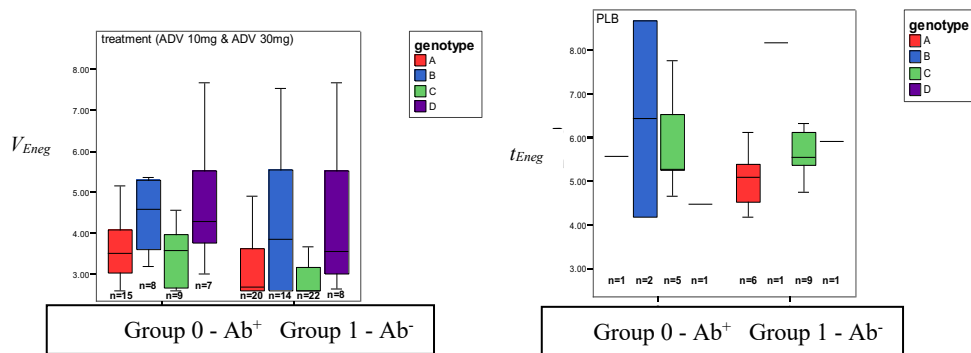


Figure 7: The comparison of genotype between the effects of placebo (PLB) (left) versus 10 mg and 30 mg doses (right) of *Adefovir* (ADV 10/30) on  $V_{Neg}$  according to Ab status at the time when HBeAg became negative.

If we examine the effects of genotype and Ab status on  $t_{Neg}$ , we see that Ab status does not influence  $t_{Neg}$  in the PLB arm (Figure 8). However, we see a big influence of Ab status on  $t_{Neg}$  in the ADV arm ( $p=0.001$ ). For all four genotypes,  $t_{Neg}$  is shorter in Group 0 than for Group 1. This means that the time to HBeAg loss is longer when antibodies are absent. This, in turn, implies that

the immune response is playing a role in expediting the time to HBeAg loss as per genotype.

When we compare the PLB and ADV arms (combined 10 and 30 mg), we see that  $t_{Neg}$  is shorter in the PLB arm when we compare Groups 0 and 1. For example, for genotype C, Group 0,  $t_{Neg}$  is notably earlier in PLB than in Group 0 ADV. We also see that in the ADV arm that  $t_{Neg}$  is notably earlier in Group 0 than in Group 1 ( $p=0.001$ ). Statistically, genotypes A, B and D give different  $t_{Neg}$  ( $p=0.003$ ,  $0.003$  and  $0.05$ , respectively) between Groups 0 and 1.

This implies that antibody status is more influential than genotype in determining  $t_{Neg}$ . Therefore, we can assume that the presence of antibodies in the context of treatment induces earlier loss of HBeAg for each genotype.

In a recent study to investigate genotype impact on the long-term virological outcome of chronic HBV infection it was found that interferon-induced loss of HBeAg was seen in 44% of patients with genotype C, as compared with 92% with non-C genotypes after a median of 9.2 years of follow-up [48].

Highly active genotype C infection often remained highly active. We did not investigate the ratio of HBeAg<sup>+</sup> versus HBeAg<sup>-</sup> patients as per genotype but based on this recent new finding, further investigation is warranted on this particular genotype for this data set.

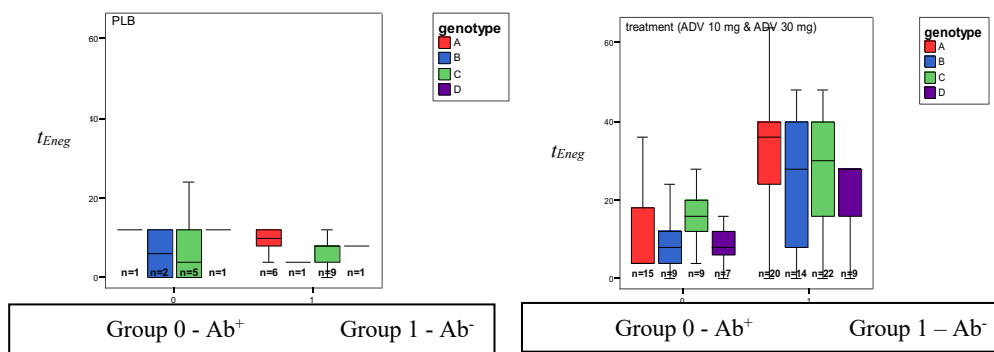


Figure 8: The comparison of genotype between the effects of placebo (PLB) (left) versus 10 mg and 30 mg doses (right) of *Adefovir* (ADV 10/30) on  $t_{Eneq}$  according to Ab status at the time when HBeAg became negative.

Our earlier prediction of earlier occurrence of a lower  $V_{Eneq}$  in Ab<sup>+</sup> individuals was half-true in that we indeed observed earlier occurrence of  $V_{Eneq}$  in Ab<sup>+</sup> individuals but it was not significant. Among all patients, some became HBeAg negative while others did not. Based on these findings we can claim that treatment significantly influences the number of patients that experience HBeAg loss.

There was an influence of HBeAg loss on the 1<sup>st</sup> and 2<sup>nd</sup> slopes (Figure 9). Patients that became HBeAg negative, had significantly steeper 1<sup>st</sup> slope (30% 1<sup>st</sup> slope  $< -2.5$  log/wk) than those that did not become HBeAg negative (13% 1<sup>st</sup> slope  $< -2.5$  log/wk) (Fischer exact  $p < 0.005$ ). Patients that became HBeAg negative, had also significantly steeper 2<sup>nd</sup> slope (17% 2<sup>nd</sup> slope  $< -0.3$  log/wk) than those that did not become HBeAg negative (8% 2<sup>nd</sup> slope  $< -0.3$  log/wk) (Fischer exact test  $p < 0.05$ ). However, the Ab status at  $t_{Eneq}$  (group AB0 or AB1) had no direct influence on the 1<sup>st</sup> and 2<sup>nd</sup> slope. AB0 patients had both

significantly earlier  $t_{Neg}$  (ADV-10 MW  $p=0.010$ , ADV-30 MW  $p<0.0005$ ) and higher  $V_{Neg}$  within treatment groups (ADV-10 MW  $p=0.031$ , ADV-30 MW  $p<0.0005$ ). No such correlations were found in PLB group.

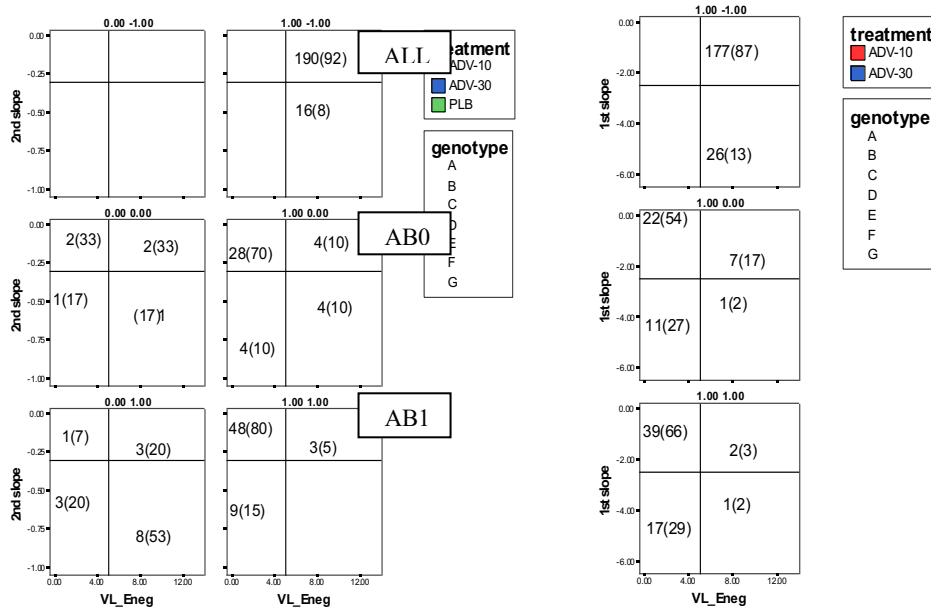


Figure 9: Scatterplots showing the relationship between 1<sup>st</sup> slopes (left) and 2<sup>nd</sup> slopes (right) and  $V_{L\_Eneg}$  in the context of treatment dose. Note there is no 1<sup>st</sup> slope in PLB patients.

### 3.3.2 The model

The model is a system of ODEs with four variables and includes the uninfected cell, infected cell, HBeAg and free virus populations. The schematic diagram follows and illustrates the interactions between the variables.

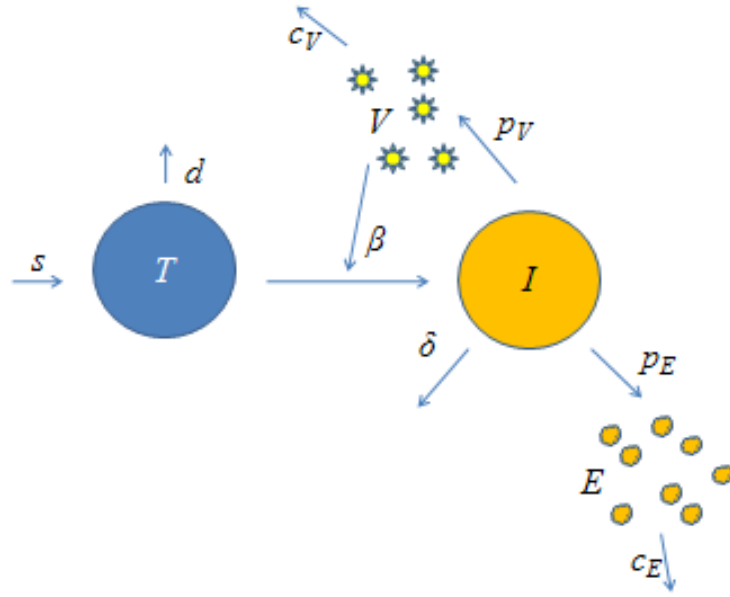


Figure 10: Schematic diagram of 4D model of HBV infection with HBeAg as a model variable

The model follows directly from the schematic and is an extension of the basic model of HBV dynamics [65].

$$\frac{dT}{dt} = s - \beta VT - dT$$

$$\frac{dI}{dt} = \beta VT - \delta(1 + (m-1)I_c/(\theta + I_c))I_c$$

$$\frac{dE}{dt} = p_E I_c - c_E E$$

$$\frac{dV}{dt} = (1 - \epsilon)p_V I_c - c_V V$$

The uninfected hepatocytes have a constant influx into the system at rate  $s$ . They also leave the system by natural causes at rate  $d$ . Hepatocytes that become infected leave the uninfected cell compartment to join the infected cell

compartment at rate  $\beta$ . Initially, the cells become infected to carry cccDNA and die by natural causes at constant rate  $\delta$ . We include the expression  $(1+(m-1)I_c/(\theta+I_c))$ , where  $m$  is a constant and  $I_c/(\theta+I_c)$  is a saturation function, to represent the effects of the immune response. This expression is a function of  $\delta$ . In the absence of an effective immune response,  $m=1$  and the equation for  $I_c$  becomes  $dI_c/dt = \beta VT - \delta I_c$ . Infected hepatocytes carrying cccDNA are capable of producing virus and also the HBeAg. It should be noted here that the immune response in a biological setting does not simply comprise antibodies. The cellular arm of the immune system is also presumed to be active and hypothetically has far greater effect on reducing the number of infected cells via HBV-specific effector T cells (killer T cells) than antibodies would. Thus, realistically, our parameter  $m$  represents not just the active antibodies but the cellular arm of the immune system as well. The HBeAg is produced by the infected hepatocytes carrying cccDNA at rate  $p_E$  and also are removed naturally at constant rate  $c_E$ . The virus comes into the system from the infected hepatocytes carrying cccDNA at constant rate  $p_V$  and natural clearance of free virus occurs at constant rate  $c_V$ . Treatment is introduced in the form of a polymerase inhibitor, represented by the term  $(1-\varepsilon)$  and acts to lower the production rate of virus. If  $\varepsilon=1$ , then the polymerase inhibitor is 100% effective.

A condition is placed on the system whereby an output variable  $E_{pos}$  is equal to 0 if the HBeAg is undetectable below a threshold  $E_x$ , i.e.  $E < E_x$ , and  $E_{pos}$  is equal to 1 if the HBeAg is detectable, i.e.  $E \geq E_x$ . This is done because the clinical data set reflects whether an individual either had detectable HBeAg ( $E_{pos}=1$  for  $E \geq E_x$ ) or not ( $E_{pos}=0$  for  $E < E_x$ ), where  $E_x$  is the assay limit of detection. An

individual was classified as having responded to treatment successfully if they had 2 consecutive points with either HBV-DNA < 1000 copies/ml plasma or with negative HBeAg. In this way, we approach the analysis of HBeAg kinetics in a qualitative way. The limit of detection for HBeAg,  $E_x$ , was assigned a value based on estimated HBeAg levels (pre-negativity) during treatment in a chronic HBV-infected setting.

The fact that the HBeAg population originates from the cccDNA-infected cell population and not directly from the virus population adds a level of specificity: we can test our theory pertaining to HBeAg loss being a function of cccDNA-infected cell loss rather than viral load decay and also confirm observations from data. The treatment parameter  $\varepsilon$  (for the model) has no direct effect on  $E$  (the population of HBeAg in the model): it acts to modify the production rate of virus instantly decreasing its value when  $\varepsilon > 0$ . Thus, fewer virions are produced while the same amount is being cleared. This is why the viral load decreases. Since fewer virions are produced, there are fewer virions to infect cells. This means that fewer cells get infected. If fewer cells are becoming infected, then presumably, fewer cells are producing HBeAg.

In order to run simulations using the *Madonna Berkeley* software we first solved for steady state solutions in order to use them as initial conditions. In the case of this four-dimensional model, there is one stable fixed point. We set the initial condition for  $V$  at a pre-treatment value according to mean VL0 values seen in data. We also rewrite one of the parameters, in this case  $d$ , in terms of the value of  $V_0$ . All other initial conditions are written in terms of the other parameters.

### **Viral kinetics with PLB**

To simulate the effects of PLB, we assume that the virus, infected cell and HBeAg populations are in steady state before treatment. Thus the levels of  $T_0$ ,  $I_{c0}$ ,  $E_0$  and  $V_0$  are related by setting all initial populations to 0 ( $\varepsilon=0$ ,  $m=1$ ). For kinetic simulations, we initialize the system using the pre-calculated steady state solutions as initial conditions and we set  $V_0$  at  $V_0=1\times 10^{10}$  since it is a reasonable approximation of the pre-treatment virus load during chronic infection. We then solve the equation  $dT/dt$  for a chosen parameter ( $d$ ) having substituted the value for  $V_0$  for  $V$  in the  $dT/dt$  equation. The system is in pre-treatment steady state: the chronic phase of infection.

We assigned progressively higher values to  $m$  while maintaining  $\varepsilon=0$ . (Initially, the system is in chronic steady state where  $m=1$  and  $\varepsilon=0$ .) We observed that higher values of  $m$  yielded slightly earlier  $t_{Neg}$ . However, for progressively higher values of  $m$ ,  $V_{Neg}$  remained the same. This finding mirrors what was observed in the data. If we equate the potency of  $m$  to the presence or absence of antibodies (AB0/AB1) then mathematical simulations provide evidence to support the data: in the case of the PLB arm, both  $V_{Neg}$  and  $t_{Neg}$  are independent of antibody status.

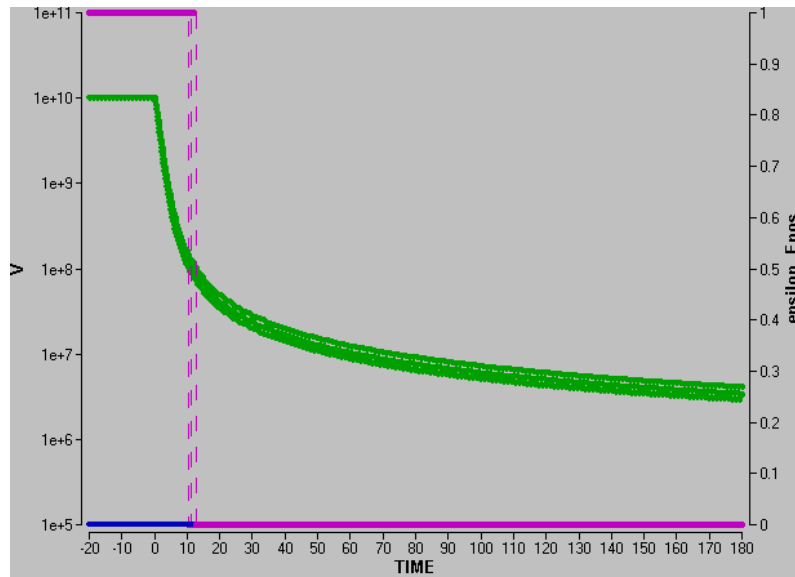


Figure 11: The effects of different values of  $m$ :  $m=6, 7$  and  $8$ . Higher values for  $m$  do not result in changes in  $V_{Neg}$  or  $t_{Neg}$ . The viral load trajectories are seen in green while the  $V_{Neg}$  vertices are seen in pink.

This result provides evidence that HBeAg levels are independent of HBeAb antibody status in the context of a PLB setting, or in the case of the model, when  $\varepsilon=0$ . Even though  $m$  induces viral load decline and a reduction in HBeAg levels to induce HBeAg negativity, the quantitative differences between the respective changes in  $V, I$  (not shown) and  $E$  (not shown) do not vary dramatically between  $m$  values.

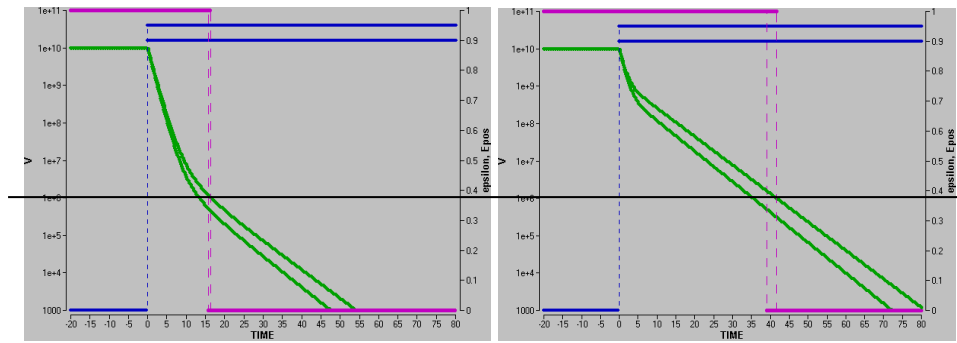
### Viral kinetics with ADV

To simulate the effects of treatment, we assume that the virus, infected cell and HBeAg populations are in chronic steady state before treatment. To assess the effects of different treatment efficacies we chose  $\varepsilon=0.9$  and  $0.95$  to coincide with the doses of ADV at 10 mg and 30 mg. With higher potency of treatment the virus, infected cell and HBeAg populations decay to progressively lower

values (Figures 12, 13). The virus population decays in a biphasic manner. This is typical (previously reported for basic model [31, 65, 66]) behavior and reflects the  $\varepsilon$  (treatment) and  $\delta$  (infected cell loss) phases of decay. When treatment is introduced ( $t=0$ ), the virus load immediately begins to decay. The length and magnitude of viral load decay is governed by the equation  $V(t)=V_0(1-\varepsilon+\varepsilon e^{-ct})$ . In the first phase called the  $\varepsilon$ -phase (1<sup>st</sup> slope), the virus load drops to a lower level and accordingly, the infected cell and HBeAg populations begin to decay as well.

According to the model in the case where there is an absence of an immune response,  $m=1$ , (equating to an absence/low level of antibodies/AB1), HBeAg becomes negative at an earlier time point ( $t_{Neg}$ ) when  $\varepsilon$  is higher (Figure 12 b)). The viral load is slightly lower for a higher value of  $\varepsilon$ . In the presence of an immune response during treatment, we see a different story in terms of  $t_{Neg}$  (Figure 12 a)). The viral load is slightly lower for a higher value of  $\varepsilon$  but HBeAg becomes negative at the same time meaning the potency of treatment does influence  $t_{Neg}$  in the context of an effective immune response where  $m>1$  (equating to presence/ detectable level of antibodies/AB0).

Interestingly, if we compare the AB1 and AB0 cases, we see that there is no difference between  $V_{Neg}$  but  $t_{Neg}$  is considerably earlier for both values of  $\varepsilon$  in the AB0 case. This is precisely what the data indicate. This implies a pathologically constructive role of the immune response/antibodies.



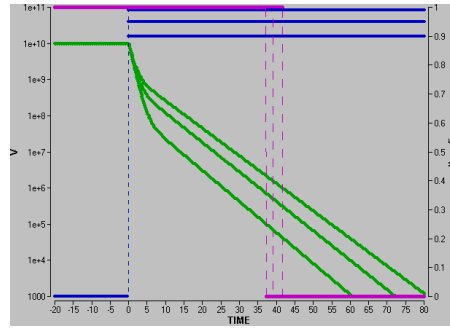
a) AB0

b) AB1

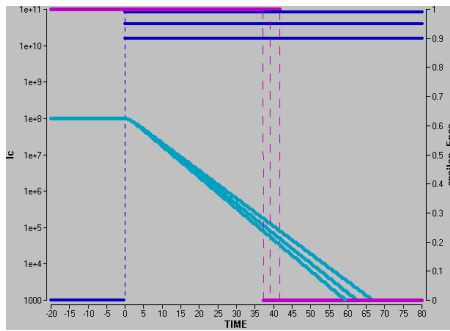
Figure 12: Time series plots showing effects of different  $\varepsilon$ . a) shows the effects of treatment in the presence of an immune response (AB0)  $\varepsilon=0.9; 0.95$ ,  $m=4$ ; and b) shows the effects of treatment in the absence of an immune response (AB1)  $\varepsilon=0.9; 0.95$ ,  $m=1$  where  $V$  (green) is the viral load trajectory and the vertical purple dotted lines are the intersection lines indicative of  $V_{Eneg}$ .

The second phase of decay (the  $\delta$ -phase (2<sup>nd</sup> slope)), has the same slope for both  $\varepsilon$  values. It is function of  $\varepsilon$  whereby the slope is determined by  $\varepsilon \times \delta$ . The  $\delta$ -phase of decay spans a longer period of time than the  $\varepsilon$ -phase. During the  $\delta$ -phase, the virus load drops to progressively lower levels.

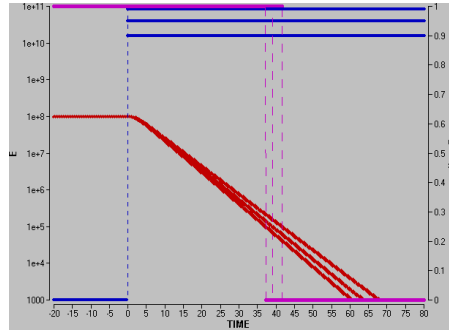
Figure 13 demonstrates the decay behaviours of the infected cell and HBeAg populations in accordance with viral load decay for three progressively larger values of  $\varepsilon$ . The infected cell and HBeAg populations decay with a single exponential (the decay is monophasic).



a)  $V$



b)  $I_c$



c)  $E$

Figure 13: Time-series simulations showing the effects of  $\varepsilon$  at values 0.9, 0.95 and 0.99 on  $V$  (a)),  $I_c$  (b)) and  $E$  (c)) trajectories. The purple vertical dotted lines represent the transition to HBeAg negativity.

The HBeAg becomes undetectable at progressively lower viral loads with increasing  $\varepsilon$ . This is simply due to the differences in the  $\varepsilon$ -phases induced by the differences in  $\varepsilon$ . The decay curves for  $I_c$  and  $E$  are virtually identical which is somewhat intuitive since  $E$  is a direct by-product of  $I_c$  and  $I_c$  is indirectly influenced by  $\varepsilon$ .

## Comparison of viral kinetics of PLB with ADV

When we compared the effects of PLB with ADV, that is, when we assign  $\varepsilon$  and  $m$  different combinations of values, we see precisely what we saw in the data. In the case where treatment is absent ( $\varepsilon=0$ ) with an adequate immune response ( $m=4$ ), we see that the HBeAg loss occurs at an earlier time. However, the viral load is higher at  $t_{Neg}$  than when treatment is present ( $\varepsilon=0.9$ ) and an immune response is weak ( $m=1$ ). It is clear why this occurs from Figure 14. The viral load decays more rapidly in the case where only an effective immune response is present resulting in a more rapid decay in viral load (and subsequently in the number of infected cells and HBeAg) inducing HBeAg loss at an earlier time. Since it occurs early, the viral load is subsequently higher due to the fact that it hasn't had enough time to decay to a lower level.

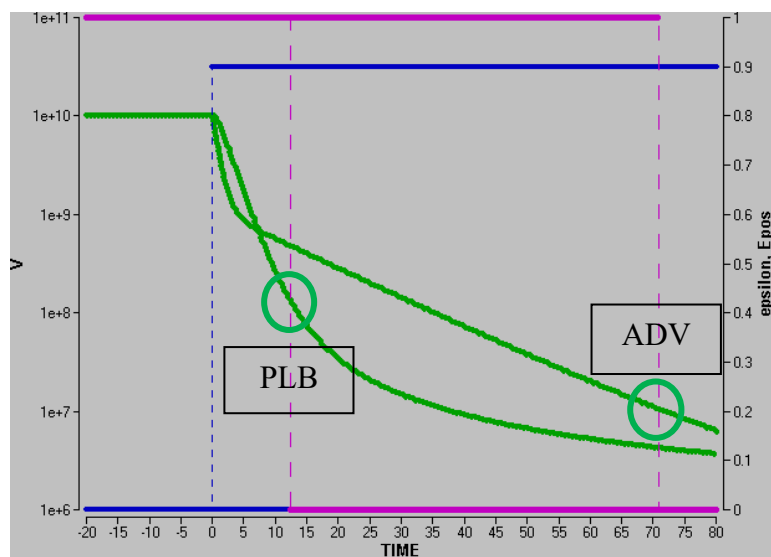


Figure 14: Comparison of  $V_{Neg}$  and  $t_{Neg}$  with treatment versus with PLB.

Viral load trajectories are seen in green with  $V_{Neg}$  and  $t_{Neg}$  vertices marked with green circles.  $V_{Neg}$  is lower and occurs later ( $t_{Neg}$ ) in the case where  $\varepsilon=0.9$ ;  $m=1$  (ADV 10) as compared with the case where  $\varepsilon=0$ ;  $m=4$  (PLB).

As previously mentioned, some patients do not become HBeAg negative but they do experience viral load decay to undetectable levels. The conditions under which HBeAg becomes negative can also be tested using the model. According to the model, it can occur for a certain set of mathematical parameters. For example, we can simulate a situation where the viral load decay patterns are almost identical but the HBeAg decay patterns are completely different (Figure 15). For example when the loss rate of HBeAg is higher, the HBeAg decays much faster without having an effect on the viral load decay pattern. This is dependent on the HBeAg loss rate. The infected cell population decay pattern is the same for different HBeAg loss rates (not shown).

It should be noted that the loss rate of HBeAg might accelerate according to the loss rate of cccDNA/per infected cell. So it is plausible that treatment which has been shown to induce cccDNA loss causes an increase in the loss of HBeAg perhaps resulting in a switch to HBeAg negative status but not affecting the absolute number of infected cells or the viral load decay (to undetectable levels). Figure 15 shows two superimposed time series simulations where the viral load (seen in green) declines in exactly the same manner and rate whilst HBeAg (red) declines in two completely different manners and rates. In one case, HBeAg declines rapidly to change status from positive to negative as indicated by the dotted vertical pink line and in the other case, it remains positive as indicated by the continuous horizontal pink line. Hypothetically, if a patient had a combination of pathological features that promoted a slower loss of cccDNA as per infected cell, then it is possible that their HBeAg status would remain

positive for a longer period of time irrespective of the effects of treatment in the viral load.

Future work may involve development of the model to incorporate an intracellular component that accounts for the cccDNA population as per infected cell. Then we could investigate how this population changes according to changes in treatment efficacy and immune response potency. This will be discussed further in the discussion in Chapter 5.

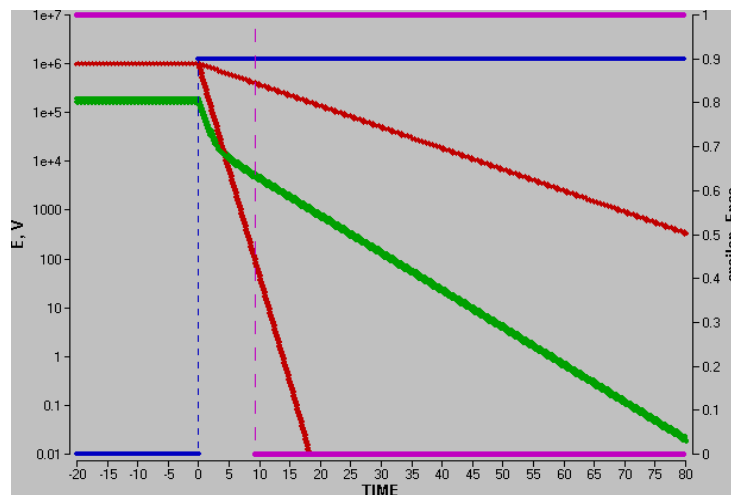


Figure 15: Two scenarios depicting virtually identical viral load decay patterns (green) with 2 different HBeAg decay patterns. In one case, the HBeAg becomes negative (as indicated by the appearance of the pink dotted vertical line). This is due to a difference in the loss rate of HBeAg.

We also investigated whether or not the initial viral load (VL0) or the initial level of HBeAg (E0) affected or determined HBeAg status and/or decay. That is, whether the initial amount of virus and/or HBeAg causes a switch in HBeAg status from positive to negative. We found that  $V_{Eneg}$  and  $t_{Eneg}$  were not

influenced whatsoever by a difference in VL0 (Figure 16 a)) but that both  $V_{Neg}$  and  $t_{Neg}$  were highly influenced by a difference in E0 (Figure 16 b)). This makes sense in that the decay curves for the viral load for two different E0 remain the same in the context of E decay curves that differ only by initial condition.

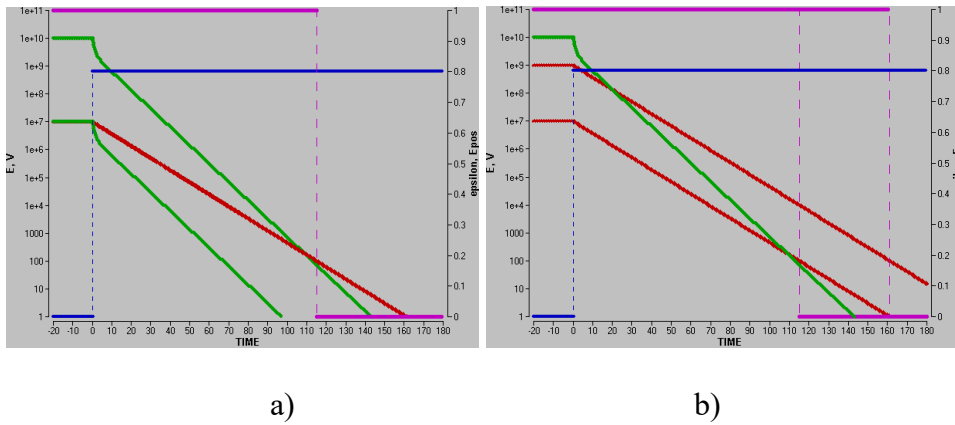


Figure 16: The effects of different VL0 (a) and E0 (b). In the VL0 case ( $V_0=1e^{10}$  vs.  $1e^7$ ), the HBeAg becomes negative (as indicated by the appearance of the pink dotted vertical line) at exactly the same VL and time. In the E0 case ( $E_0=1e^9$  vs.  $1e^7$ ), the HBeAg becomes negative at different times and for different viral loads.

## Chapter 4

### Novel decay dynamics revealed for virus mediated drug activation in cytomegalovirus infection<sup>16</sup>

#### 4.1 Introduction

The herpes virus CMV has co-evolved with humans over many millennia and is well adapted to the immunocompetent host. However, in a variety of immune deficient hosts including the neonate, organ transplant recipients, patients with common variable immune deficiency and HIV-infected patients the virus can cause life-threatening pathologies. The synthetic nucleoside analogue *Ganciclovir* (GCV) has become the antiviral drug of choice for controlling CMV infection and disease. Cytomegalovirus remains an important cause of morbidity in a variety of immunocompromised hosts and has a significant economic impact on general healthcare costs. Despite recent encouraging results, there is no licensed vaccine against CMV. Consequently, the mainstay of control has been through antiviral chemotherapy predominantly with GCV or its valine ester VGCV. The drug can be deployed prophylactically, pre-emptively or for therapy of overt CMV infection and disease. In the present study, we have utilized frequent viral load data over the first 21 days of therapy in patients with a single CMV genotype (one of gB1, gB2, gB3 or gB4) who

---

<sup>16</sup> Chapter 4 focuses on a paper that will be submitted for publication in July of 2012 and explores the intracellular feedback loop between an anti-CMV drug *Valganciclovir* and CMV itself.

were enrolled in the VICTOR clinical trial testing the safety and efficacy of GCV versus VGCV in solid organ transplant patients with CMV disease. Because viral load decay patterns in the context of antiviral treatment in patients with CMV disease were so highly dynamic, we developed a new classification method for patients according to their specific kinetic profile patterns based on differences between the early decline phase (between days 0 and 3), the 2<sup>nd</sup> phase (between days 7 and 21 or 14 and 21) and the ‘hump’ phase (between days 3 and 7 or 7 and 14).

#### **4.2 VICTOR study and classifications**

The VICTOR study included patients who were solid organ recipients and most had CMV disease at the time of enrolment. This 2 arm study evaluated the efficacy and safety of oral *valganciclovir* (Valcyte) compared with intravenous ganciclovir for the treatment of CMV disease in solid organ transplant recipients. Eligible patients were randomized to receive either 1) Valcyte (VGCV) 900mg po bid or 2) Ganciclovir (GCV) 5mg/kg iv bid for 21 days and then both arms continued with maintenance GCV at a 900 mg daily dose of VGCV until day 49 [3].<sup>17</sup> We examined both arms and found no difference in viral kinetics between the arms and thus analyzed the data as a whole. Viral loads were taken at days 0, 3, 7, 14 and 21 in the case of whole blood (WB) sampling and days 0, 3, 7, 10, 14, 17, 21 and 49 in the case of plasma sampling. For the purposes of this chapter, we only included the analysis from the WB data and patients in whom a single gB genotype infection was present. Consequently, we analyzed a total of 92 patients out of a total of 113. The

---

<sup>17</sup> <http://clinicaltrials.gov/ct2/show/NCT00431353>

patients omitted from the analysis were missing vital viral load data such as day 3 or day 21, for example. Data was plotted as time series plots to assess the kinetic characteristics qualitatively. Patients with drug resistance mutations were excluded from the analysis.

The four kinetic profiles were assigned based upon kinetics over the first 21 days of therapy and a patient was classified as having a 'Hump' (HM) profile if the 1<sup>st</sup> phase slope was declining more than 0.5 logs, the hump slope was either 0 or positive and the 2<sup>nd</sup> slope was declining. A Biphasic (BP) profile is similar to the HM profile with the exception of the lack of a hump phase; i.e. rapid viral load decline between days 0-3 followed by continuous decline from day 3 onward. A Delay (DL) profile was defined by a 1<sup>st</sup> phase slope of <0.5 logs between days 0-3 followed by a continuous decline, and a Rebound (RB) profile was defined by an initial rapid decline between days 0-7 followed by continued increase in viral load in the 2<sup>nd</sup> phase as opposed to decline. Notably, the Hump kinetic pattern has not previously been observed in other viral kinetics studies and thus prompted deeper analysis of why these patterns exist and at high frequencies.

## **4.3 Results**

### **4.3.1 Viral kinetic analysis**

The categories include Hump (HM), Biphasic (BP), Delay (DL) and Rebound (RB). Interestingly, the HM profile occurred at a very high frequency: more than 60% of patients manifested this profile. Below is a table showing the distributions of factors for each profile as determined from the data.

Viral Kinetic Property	Viral Kinetics (VK) Pattern			
	Hump (HM)	Bi-Phasic (BP)	Delayed (DL)	Rebound (RB)
(Mean ± Stdev)				
Patients per VK-pattern N (%)	56 (61%)	18 (20%)	14 (15%)	4 (4%)
Baseline CMV load (log ge/ml)	5.2 ± 0.8	5.3 ± 0.9	4.3 ± 0.6 * <sup>1</sup>	6.1 ± 0.5 * <sup>2</sup>
Primary endpoint viral load (day 21)	2.6 ± 0.9	2.6 ± 0.9	2.7 ± 0.8	4.4 ± 0.1* <sup>7</sup>
1 <sup>st</sup> phase slope (log ge/ml per week)	-3.1 ± 0.1	-2.7 ± 0.2	-0.5 ± -0.5	-3.5 ± 0.7
1 <sup>st</sup> phase decline magnitude (log ge/ml)	-1.3 ± 0.4	-1.2 ± 0.6	-0.2 ± 0.2 * <sup>3</sup>	-1.5 ± 0.3
Hump magnitude (log cp/ml)	+0.1 ± 0.3 * <sup>4</sup>	-0.4+/-0.2	-0.3+/-0.4	-0.8+/-0.3
2 <sup>nd</sup> phase slope (log ge/ml per week)	-0.7 ± 0.1	-0.6 ± 0.1	-0.5 ± 0.3	+0.3 ± 0.1 * <sup>5</sup>
CMV decline at day 21 (log ge/ml)	-2.6 ± 0.7	-2.7 ± 0.6	-1.5 ± 0.7 * <sup>6</sup>	-1.7 ± 0.5

Table 1: Summary of CMV Kinetics and Viral Dynamics Model Parameters<sup>18</sup>

The HM profile is an entirely new kinetic pattern that was not previously described and consists of rapid 1<sup>st</sup> phase decline followed by a transient rise in viral load from day 3 to day 7. After day 7, the viral load declines to undetectable levels in most of the HM patients (Figure 17). Interestingly, the transient rise in viral load does not adversely affect the endpoint viral load

---

<sup>18</sup>\*1) Baseline CMV load in patients with DL is significantly ( $p < 0.001$ ) lower than that of HM, BP and RB (by definition).

\*2) Baseline CMV load in patients with RB is significantly ( $p < 0.02$ ) higher than that of HM, BP and DL (by definition).

\*3) 1<sup>st</sup> phase decline in patients with DL is significantly ( $p < 0.001$ ) lower than that of HM, BP and RB (by definition).

\*4) Slope at days 3-7 in patients with HM is significantly ( $p < 0.001$ ) different than that of BP and DL (by definition).

\*5) 2<sup>nd</sup> phase slope at days 7-21 in patients with RB is significantly ( $p < 0.001$ ) different than that of HM, BP and DL (by definition).

\*6) Total CMV magnitude decline at day 21 in patients with DL is significantly ( $p < 0.002$ ) lower than that of HM and BP (by definition).

(Table 1). A significant proportion of HM patients were gB genotype 1 (Table 1) although this relationship will not be developed further in the current work. The BP profile has been observed and reported in previous publications but in this case represents only a fraction (20%) of patient kinetic profiles. It consists of a rapid 1<sup>st</sup> phase followed by a slower 2<sup>nd</sup> phase (Figure 17).

15% of patients exhibited the DL profile characterized by a slow 1<sup>st</sup> phase (<0.5 log viral load decline in first 3 days) and a variable 2<sup>nd</sup> phase which comprised either decline or plateauing of the viral load (Figure 17). It is possible that these patients respond less dramatically to treatment because their baseline viral loads are quite low (Table 1) which may indicate an inherent mechanism operating to keep viral loads suppressed to low levels even in the absence of treatment.

The RB profile represents a small fraction of patients (4%) and consists of a rapid 1<sup>st</sup> phase decline followed by subsequent growth in the viral load at day 7 (Figure 17). These patients were assessed for the presence of drug resistance mutations in UL97 and the CMV DNA polymerase and interestingly, none were found to have documented GCV resistance mutations at either genetic loci before or after the rebound. This implies that there is something else causing the 'rebound' in viral load.

Distinctions between profile patterns were made according to statistically significant differences between slopes as per phase. For example, the slope between days 3 and 7 (hump slope) in the HM profile is significantly higher ( $p < 0.001$ ) than for the BP and DL profiles. In fact, it is positive while the others

are negative. (See footnotes for Table 1 for details.) Interestingly, we observed that the mean baseline CMV load in the DL profile was significantly lower than in the HM and BP profiles ( $p < 0.001$ ) while the baseline viral load in the RB group was significantly higher than those of the HM, BP and DL profiles. The 1<sup>st</sup> phase decline in the DL profile was also significantly lower than those of the HM, BP and RB profiles, which is a given based on the definition of DL. In addition, total CMV decline (over 21 days) in the DL group was significantly lower than for the HM and BP profiles.

Baseline viral load (VL0), magnitude of the 1<sup>st</sup> and 2<sup>nd</sup> phase declines, and total magnitude of CMV load decline between all kinetic groups were investigated further. All the patients, as a single group irrespective of their decline pattern, showed a correlation between VL0 and 1<sup>st</sup> phase decline ( $R = 0.521$ ,  $p < 0.001$ ) but only the HM group showed this correlation as a single profile ( $R = 0.414$ ,  $p < 0.001$ ). We observed a strong correlation between the 2<sup>nd</sup> phase decline and total magnitude of the viral load decline in the HM, BP and DL groups ( $R = 0.810$ ,  $p < 0.001$ ;  $R = 0.655$ ,  $p < 0.001$ ;  $R = 0.796$ ,  $p < 0.001$ ). There were also strong correlations in the HM and BP profiles in the case of total magnitude viral decline ( $R = -0.737$ ,  $p = 0.001$ ;  $R = -0.661$ ,  $p = 0.001$ ) and endpoint viral load ( $R = 0.734$ ,  $p = 0.001$ ;  $R = 0.679$ ,  $p = 0.001$ ). That is, the overall magnitude of viral load decline is predictive of the endpoint viral load in the HM and BP categories.

The HM kinetic profile is of particular interest as it occurred at a high frequency (>60% of patients) and cannot be simulated using the currently available viral dynamics models (data not shown). We reasoned that since the mode-of-action

of GCV is unique compared to current drugs used to treat HIV, HCV or HBV infection then this mode-of-action may account for the frequent observation of the HM profile. In other words, depending on the rates that dictate UL97 and GCV (triphosphate) levels, the profile will be different to yield one of the HM, BP, DL or RB viral kinetic patterns.

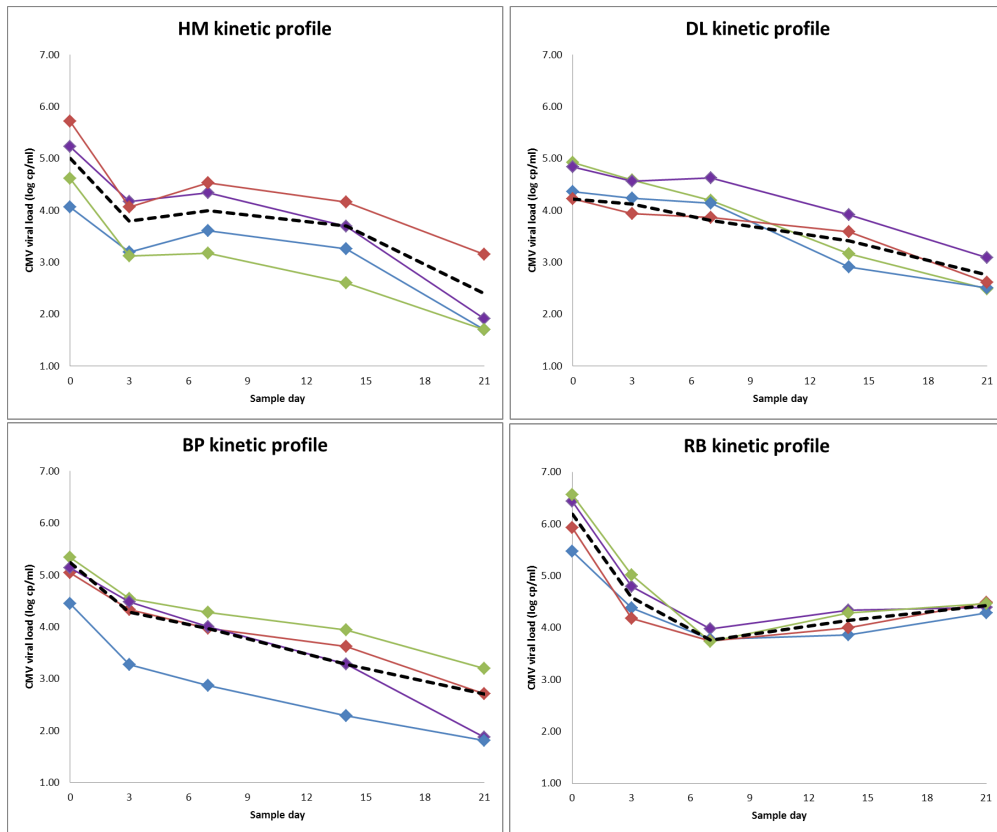


Figure 17: Data (VK – no mathematical fits) – 4 kinetic profile patterns for single genotype data set. VK for all 4 profiles in 4 single randomly-selected patients show distinct differences in profiles. The black dashed line represents the mean VL as per pattern.

Briefly, CMV transcription occurs in 3 stages: early, intermediate and late with DNA replication occurring after early transcription and via the production of a concatemeric structure that is then cleaved and packaged into new virions. [24,

25, 26, 27]. GCV triphosphate (GCVTP) interrupts this process by inhibiting viral DNA replication. We assume that this occurs at the lengthening stage: the drug inhibits lengthening of the viral DNA so that the precursor DNA for packaging is ultimately not produced. Studies have shown that GCV triphosphate levels are at least 100-fold greater in CMV-infected cells than in non-infected cells [54, 67, 71].

A central tenet of our approach to CMV replication dynamics hinges on the potential for a feedback loop between GCV and UL97. Since reduced UL97 expression occurs in the presence of GCV, and UL97, although a virion component, is transcribed as an early-late gene that likely requires DNA replication for maximum expression [54] we hypothesized that during GCV treatment, UL97 levels change according to the change in intracellular replication levels and therefore this could potentially result in variability in viral load during the on-treatment timeframe. Changing replication levels would be the result of variable efficacy of  $\varepsilon$  during treatment based on changing GCVTP levels which ultimately is influenced by UL97 activity. The power in this theory is 2-fold: it is testable using mathematical modeling as a tool to model the actual clinical data (summarized in Table 1) and the results can be used to refine our understanding of the antiviral activity of GCV and other new selective anti-CMV drugs that depend on activation by UL97 or by other herpes viral homologues of UL97 or more broadly, the herpes viral thymidine kinases.

Previous estimates of decay rates of CMV viral load have been calculated under the assumption that viral decay is biphasic and exponential which in the case of

our data set, is not the case. Existing models cannot yield the HM or RB profiles observed in Figure 17 and so we saw it necessary to develop a novel mathematical model of CMV infection.

#### 4.3.2 Testing the basic model

As part of the modeling process and prior to the discovery of our theory pertaining to the drug-virus feedback loop, we attempted to model the kinetic patterns seen in data with the basic model of viral infection. Since this model is well characterized and studied, we thought it was a good starting point. To date, the basic model of infection has been able to demonstrate monophasic and biphasic decay patterns. There are many possible reasons why the HM profile would occur. Of them includes pharmacokinetic changes in anti-viral effectiveness. We tested this possibility using the basic model of infection as described in the following. When we ran time-series simulations using the basic model, we were not able to see the HM profile in a biologically plausible way.

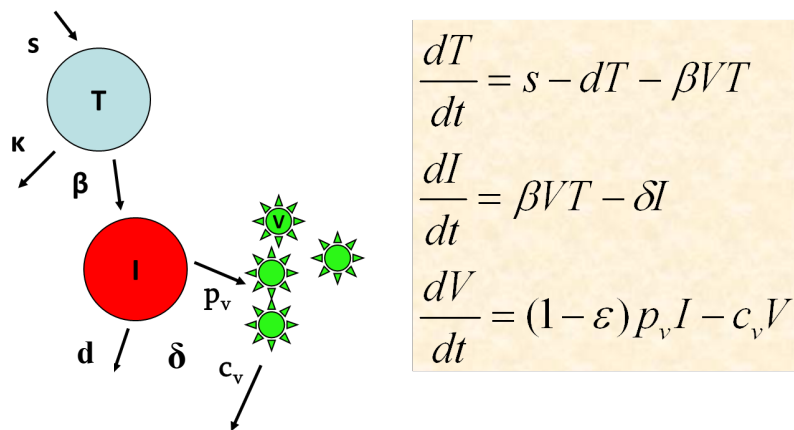


Figure 18: The basic model of infection schematic and model equations. This version of the basic model shows blocking of production of virus.

As seen in Figure 19, the only way we were able to see the HM profile was to transiently (between days 3 and 7) modify the treatment parameter or the death rate of the virus. However, there is no *a-priori* reason for either of these changes in parameters to occur.

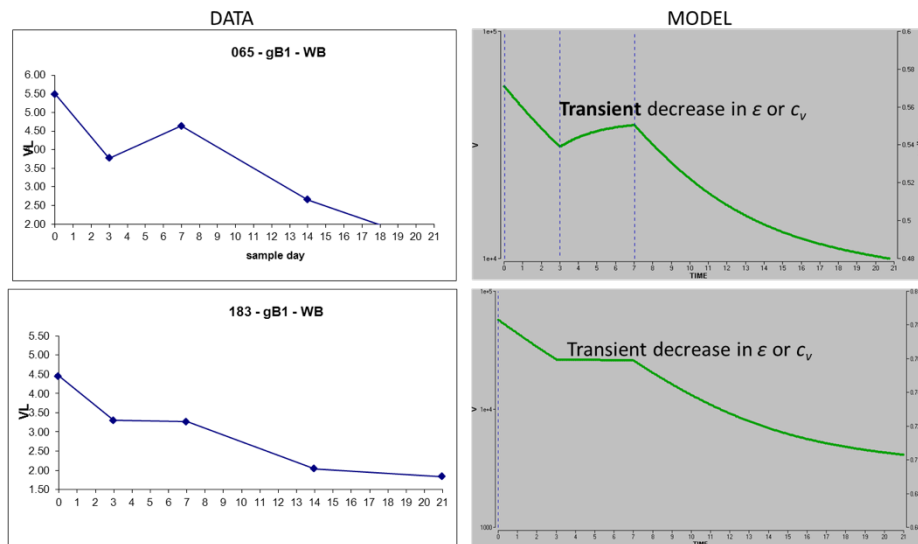


Figure 19: Time series trajectories (data versus 3D model) for 2 patients with the 2 versions of the HM profile. Pharmacokinetic changes could not be accounted for using this model.

Because GCV is taken twice daily, it is unlikely that  $\epsilon$  or  $c_v$  would change in this way. Thus, this scenario was discounted as a biologically plausible reason for the observed HM profile.

We tested many other models to test other theories as to why we see the HM profile including different cellular compartments, different physiological compartments, changes in immune response and evolution of resistance, to name a few. We developed a number of modifications of the basic viral dynamics model accordingly. However, none of these models were capable of reproducing the different viral kinetic patterns that we observed (not shown

here) and/or there was no evidence in the data to support the underlying assumptions (e.g. no resistance mutations were observed, no rapid changes in immune response observed during the first weeks of therapy, etc.). Only when we turned our thinking to intracellular modeling did we make the link between the intra-cellular relationship between CMV replication and the anti-viral effect of GCV and the HM profile were we able to develop a model that finally described all four profiles accurately.

#### **4.3.3 The novel model for GCV/CMV interaction**

Briefly,  $G_0$  is the intracellular GCV drug concentration.  $D_1$  represents the linear/circular/concatameric forms of viral DNA, and  $D_2$  represents the cleaved and packaged viral DNA. UL97 phosphorylates GCV ( $G_0$ ) to produce a mono-phosphorylated form of the drug ( $G_1$ ) which is rapidly metabolized to the active tri-phosphorylated form of the drug ( $G_3$ ) by cellular kinases. This active form of the drug then acts primarily on  $D_1$  to inhibit the prolongation of the linear DNA, formation of circular DNA and subsequent packaging of DNA for new virions. Since  $D_1$  is assumed to be the template for UL97 transcripts and hence the UL97 protein, this produces a negative-feedback loop causing the eventual reduction in both  $D_1$  and subsequently UL97 (Figure 20).

In the absence of adequate quantities of UL97, the drug, which presumably continues to enter the cell, does not get phosphorylated efficiently and so drug efficacy is reduced. This means that the viral content in the cell in the form of  $D_1$  and  $D_2$  eventually begins to rise, then peak and subsequently plateau at new

steady state levels. In addition, since  $V$  originates from  $D_2$ ,  $V$  also declines and then rises albeit, more slowly.

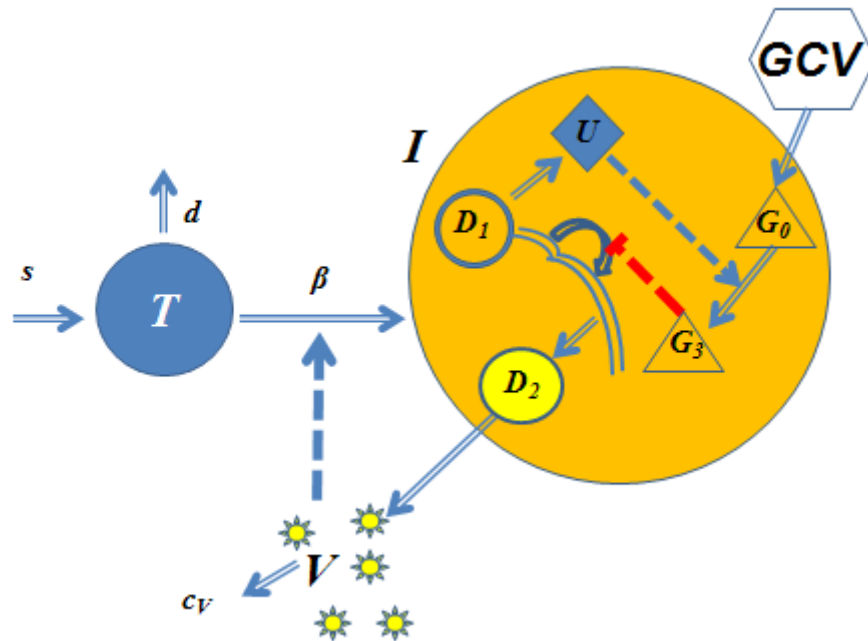


Figure 20: Schematic diagram of CMV infection process showing the negative feedback loop between UL97 and GCV. We assume is that GCV affects only the first phase directly and is directly affected by UL97 activity and presence. Once UL97 is restored to large enough quantities due to continued (amplified) viral replication, the drug is again phosphorylated, can act again, and the cycle continues. Mathematically, this could manifest as a transient rise in intracellular (cell-associated) DNA content and give rise to oscillatory behaviour.

The differential equations that follow directly from the schematic in Figure 20 are as follows.

$$dT/dt = s - dT - \beta TV$$

$$dI/dt = \beta TV - \delta I$$

$$dU/dt = gD_1 - d_u U$$

$$dG_3/dt = kUG_0 - d_G G_3$$

$$dD_1/dt = (1-\varepsilon)R_1 - \rho_1 D_1$$

$$dD_2/dt = \rho_1 D_1 - \rho_2 D_2$$

$$dV/dt = P_{frac} \rho_2 D_2 I - cV$$

The model contains seven variables that represent uninfected cells,  $T$ , infected cells,  $I$ , UL97 enzyme,  $U$ , the triphosphate form of the drug,  $G_3$ , the linear form of the viral DNA which becomes elongated for eventual cleavage into component viral parts,  $D_1$ , assembled capsid forms in which the scaffolding has been removed and replaced with viral DNA,  $D_2$ , and free virus,  $V$ . To mimic the effects of antiviral drugs we introduce a parameter,  $\varepsilon$  to reduce the production rate of  $D_1$  where  $\varepsilon = G_3^h / (\theta^h + G_3^h)$ . This equation utilizes the Hill Function which is a saturation function dependent on the value of  $h$  to dictate amount of saturation.

#### 4.3.4 Fitting the data to the novel model

Since we have measurements of viral load from whole blood (WB), we needed to translate the mathematical variables into a single variable that comprises the WB count in order to be able to compare the model findings with the data and properly fit the data to the model. Thus, we assume that  $WB = (D_1 + D_2)I + P_{frac}V$  since we assume that the amount of virus measured in WB is, for the most part, coming from intracellular DNA per infected cell as well as in part from the plasma virions.  $P_{frac}$  represents the fraction of WB that is plasma.

We ran time-series simulations using *Madonna Berkeley* software. We solved for steady state solutions and found that the system has one stable steady state. Again, we used this steady state as the initial condition to run the simulations. We set  $V$  at a pre-treatment value and solved  $\beta$  in terms of  $V$ .

We were able to accurately simulate all four kinetic profile patterns seen in data using the feedback-loop between  $U$  and  $D_1$  model (Figure 21). What is interesting, are the differences in the parameter values that yield each kinetic profile pattern. We found that on day 7 in the HM category,  $\varepsilon$  was 8% lower than on day 3 than it was on day 0. We did not find this difference in the other categories. This is strong evidence that the hump occurs due to the decrease in the amount of available phosphorylated GCV: the lack of available active drug resulting in a decrease in viral blocking and a subsequent increase in cell-associated viral load. We also observed a subsequent increase in  $\varepsilon$  by day 14: the value continues to decline in all other categories following day 7. We also found this pattern in  $G_3$ : there is 68% less  $G_3$  on day 7 than on day 3, and 8% more on day 14 than on day 7. This does not occur in any other group.  $D_1$  and  $D_2$  decline rapidly due to the effects of  $\varepsilon$  and subsequently transiently increase on or around day 3 until both reach a new steady state (not shown).

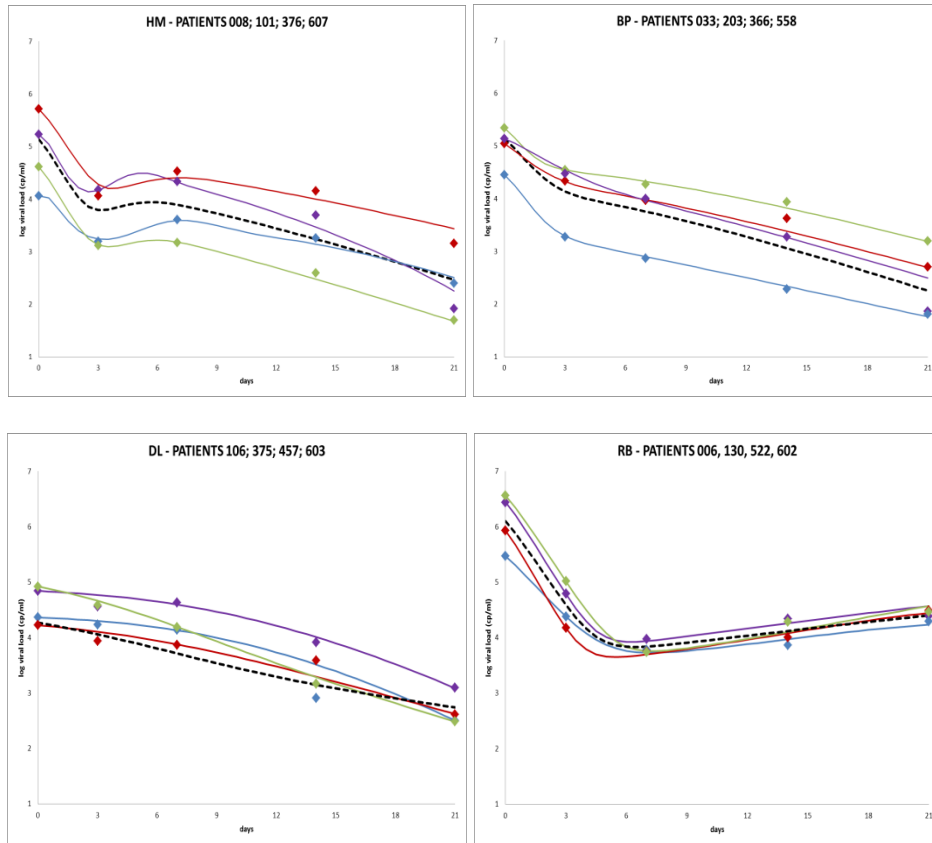


Figure 21: Mathematical simulations of 4 randomly-selected patients from each kinetic profile. The black dotted line represents the mean VL for each profile, the dots are the data points and the time series trajectories are seen in coloured solid lines.

Due to the increase in intracellular DNA in the HM profile between days 3 and 7 (both the linear/circular forms and the packaged forms) induced by decreasing levels of  $G_3$ , we see a subsequent increase in total intracellular viral load in WB. Furthermore, the infected cell population continues to decline during this phase which also affects the total WB population. Following day 7, the intracellular DNA resumes decay until day 21. Due to the combination of these factors, we see the WB viral load resume its decline at day 7 in the HM category. We predicted that UL97 expression would be reduced in the presence of GCV

revealing an inverse relationship/correlation between the variables  $U$  and  $G_3$ : that is, when  $G_3$  is higher,  $U$  should be lower. We saw exactly this in the mathematical simulations further supporting our theory (not shown).

The only qualitative or quantitative differences between the HM and CD profiles are the slopes between days 3 and 7 and 1<sup>st</sup> slope. Furthermore, since the viral load at day 0 (VL0), the endpoint viral load (VL21) and 2<sup>nd</sup> slopes are statistically similar (almost identical) between the HM and CD profiles, we used these two profiles as a comparative means to reveal the exact differences in parameters that yield these particular profiles. If our theory is correct, then the difference in profiles should be inducible by simply modifying the intracellular parameter values associated with  $U$  and  $G_3$ . The value for  $d_u$ , the decay rate for  $U$ , is highly influential with respect to the feedback loop between  $U$  and  $G_3$  and in fact, by simply modifying this and one other parameter associated with treatment efficacy, the HM profile can be seen. Interestingly, its value is higher than for the other profiles. The fact that  $d_u$  is higher means that UL97 is cleared from the system more rapidly and thus is less available for phosphorylating  $G_0$ . This would set the stage for higher viral loads in the context of high treatment efficacy and perhaps temporarily offsets the ‘decay balance’ of the system inducing a transient rise in viral load. The value of the  $d_u$  parameter is almost completely responsible for the HM profile. The only other parameter that differs between the HM and CD profiles is the Hill parameter,  $h$ , whose value partially determines the efficacy of  $\varepsilon$ . The value of  $h$  in fact dictates a change in profile pattern. Ultimately, the inter-relationship between  $d_u$  and the

treatment parameter appear to wholly define the kinetic profile patterns in WB. This provides strong evidence for our theory.

As part of our mathematical simulations and tests, we changed the value of  $d_u$  to observe the effects. When we increased the value of  $d_u$ , we saw the total amount of WB virus rise and the shape the trajectory change until eventually there is barely a hump. This is because there is less  $U$  for consumption, and therefore less  $G_3$  and a lower value for  $\varepsilon$ . Thus there is an increase in  $D_1$ ,  $D_2$  and  $V$ . When we decreased its value, we saw the viral load decay more rapidly and the shape of the trajectory change until again, there was barely a hump.

Interestingly, upon further examination, we noticed that the RB profile closely resembles the HM profile, albeit delayed. We used the model to project the behavior of the WB viral load beyond day 21 and noticed that at day 21 the viral load in the RB profile begins to decline anew. By day 90, the viral load is very close to undetectable (Figure 22). Consistent with this explanation was the finding that while plasma CMV loads at day 21 were detectable ( $>600$  cp/ml) in 100% of RB patients. This fell to 25% of RB by day 49. We checked post-primary endpoint data in plasma samples and noted that the viral load continues to decline to near undetectable levels ( $2.77$  log cp/ml by day 49). Many patients are deemed as non-responsive to GCV therapy if by day 21 the viral load is not declining or has not declined to an undetectable level. In light of this, these patients are advised to discontinue treatment due to toxicity and perceived ineffectiveness of the drug. However, if our mathematical predictions are correct, then these patients should in fact resume treatment post day 21 as it is

likely (according to our findings) that the viral load will begin to decay perhaps to eventually become undetectable. This will be elaborated on in Chapter 6.

To try to understand exactly why we see the unique profiles, we examined the effects of changing each parameter, alone and in tandem with others for each profile. We found that some parameters **dictate** the profile patterns while others simply **promote** them. +++ (---) denotes a parameter for which an increase (decrease) in its value **dictates** a change to the respective VK pattern. + (-) denotes a parameter for which an increase (decrease) in its value **promotes** a change to the respective pattern, usually in combination with other parameter changes. \* denotes a parameter for which changes in its value change the characteristics (e.g. earlier or later hump) of the respective pattern. A delay (DL) pattern can be obtained with 2 optional setups: either  $R_1$  is very small (1) or  $\rho_1$  and  $\rho_2$  are small (2). We believe that the  $R_1$  small configuration is the most plausible since the mean VL0 for these patients is low which corresponds to low  $R_1$  and  $\rho_1$  values and high  $\rho_2$  values. See Table 2.

<i>Parameter</i>	CD → HM	CD → DL	HM → RB
$R_1$		--- <sup>1</sup>	
$\rho_1$	+++	--- <sup>2</sup>	
$\rho_2$	+	--- <sup>2</sup>	
$H$	+++	+ <sup>1</sup>	
$S$			
$D$			
$A$			---
$K$			
$G$			
$Du$	+ *		- *
$G_0$			
$Dg$	+		
$\theta$			
$C$			
$Pfrac$			

Table 2: Parameters affecting the various CMV viral kinetic patterns

#### 4.4 Dose effect

Lastly we investigated what effects, if any, a lower or higher treatment dose has on the variable trajectories for each kinetic profile. We changed the value of the  $h$  function to subsequently alter the value of  $\varepsilon$  to both higher and lower values and superimposed the resulting variable trajectories against the original trajectory for each profile (Figure 22). The most important observation we made was for the RB profile. We extended the timeline to explore what happens if we extended the duration of treatment longer than 49 days: the end of treatment period in the VICTOR clinical trial. According to the model, for the RB profile the WB viral load not only ceases to increase post day 21, but actually begins to decay. Thus, according to this prediction, in a clinical setting it would be advisable for patients with the RB profile to continue treatment post day 21 in spite of the fact that it appears as though the viral load may continue to increase. This prediction is corroborated by the plasma viral load measurements for the RB patients at day 49 and 84. The second important observation for the patients with the RB profile is that giving a higher dose will not induce more rapid viral load decline. In fact, even a lower dose post day 21 would yield a modest decay trend in the viral load but a higher dose will not make it significantly faster.

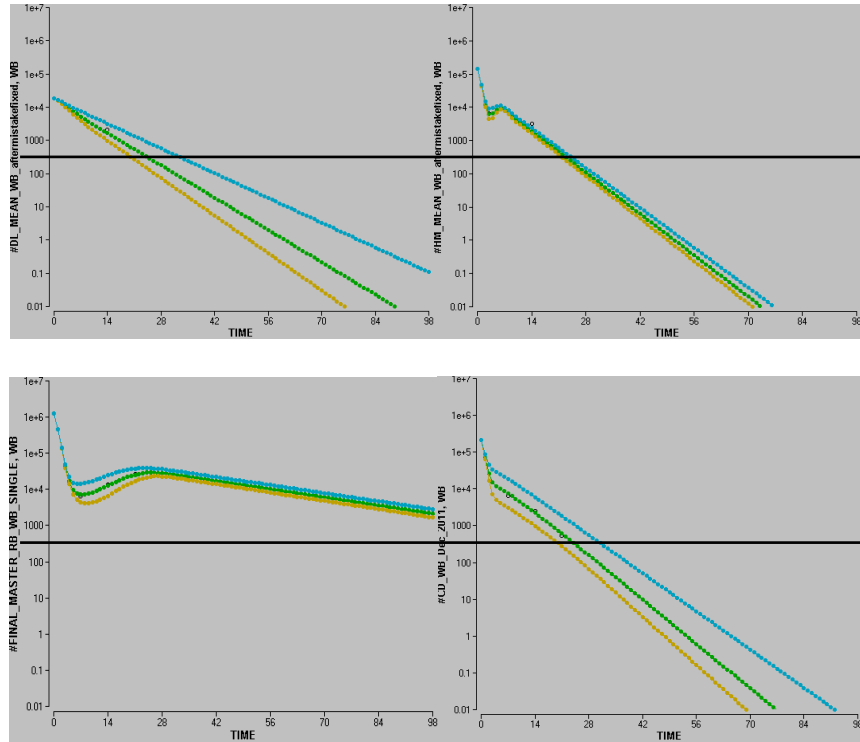


Figure 22: Effect of dosing on variable trajectories on each kinetic profile group. The variable trajectories represent the respective paths for 3 different values of  $\varepsilon$ . The black horizontal line represents the limit of detection of the viral load (600 cp/ml) and the black vertical line marks day 21.

In the case of the HM profile, there is no real affect of dose. Thus, according to the model, a lower dose would be satisfactory to yield the same decay pattern and low/undetectable viral load by day 21 and post day 21. In the case of the BP profile, a lower or higher dose actually has a more noticeable effect even within the first 21 days. There is a difference in the first phase kinetics (they are slower for a lower dose) which delays the point at which the viral load will become undetectable. This is clinically relevant as it might be advisable to increase the dose for patients manifesting the BP profile. Importantly, the viral

load does eventually become undetectable for all three doses, just at slightly different times.

For the DL case, there is also a notable difference in the variable trajectories based on dose but note that we do not see this difference until after day 21. The slope of the decay curve is steeper for a higher dose to yield more than a 1 log difference in viral load by day 42. Clinically, this may not be vital since patients with the DL profile have a more desirable prognosis, to a large extent due to significantly lower baseline viral loads. However, since the prognosis is favorable, a lower dose may be advisable from the beginning of treatment.

#### 4.5 Kinetic pattern associated with CMV genotype

We are currently continuing our investigations of the VICTOR data to determine whether or not genotype is a factor in determining the kinetic profile pattern. Table 3 shows the distribution of the kinetic profile patterns as per genotype. The fraction of gB1 patients with a hump (HM) is significantly ( $p < 0.001$ ) larger than that of other CMV genotypes.

GENOTYPE	N (% of all)	HM	BP	DL	RB
gB1	42 (45.7%)	29 (69.0%) * <sup>1</sup>	6 (14.3%)	7 (16.7%)	0 (0.0%)
gB2	16 (17.4%)	6 (37.5%)	7 (43.8%)	2 (12.5%)	1 (6.3%)
gB3	22 (23.9%)	9 (40.9%)	8 (36.4%)	3 (13.6%)	2 (9.1%)

gB4	12 (13.0%)	5 (41.7%)	4 (33.3%)	2 (16.7%)	1 (8.3%)
<b>ALL</b>	<b>92</b>	<b>49</b>	<b>25</b>	<b>14</b>	<b>4</b>

Table 3: Distribution of Viral Kinetics Pattern per CMV Genotype

We do not develop this idea further in this work due to time constraints but thought it crucial to mention as part of our continuing efforts. This will be the subject of a subsequent publication.

## Chapter 5

### **Human cytomegalovirus kinetics following institution of Artesunate after hematopoietic stem cell transplantation<sup>19</sup>**

We examined data gathered from 6 post-hematopoietic stem cell transplant (HSCT) patients with CMV drug resistant infection upon administration of an anti-malarial drug called Artesunate that has previously shown promise in the context of a CMV disease in a transplantation setting. This study showed the 2 out of 6 patients responded favorably to pre-emptive treatment with ART as determined by rapid viral decline post-administration. One of the main conclusions of the study showed that rapid viral response is thought to be a function of lower initial viral load. A simple linear model was used in this study and we did not participate in this particular aspect.

#### **5.1 Introduction**

The anti-malaria drug ART has been shown to be an effective inhibitor of cytomegalovirus (CMV) *in vitro*, in an experimental animal model, and in a recent single-case clinical use. In this first case-series of 6 stem cell transplant recipients who received preemptive ART treatment for CMV infection, we have examined the viral kinetics following institution of ART, and employed first-phase viral kinetics studies to calculate its antiviral effectiveness. Two patients demonstrated a rapid 0.8–2.1 log viral load decline by 7 days, with a viral decay half-life of 0.9–1.9 days. Four patients demonstrated a continued yet stalled

---

<sup>19</sup> Chapter 5 focuses on a paper that was published last year and is an investigation of the effects of an anti-malarial drug Artesunate on CMV.

viral growth slope during treatment. No adverse events were noted in treatment courses of up to 28 days. Overall, a divergent antiviral efficacy was revealed, ranging from 43% to 90%, which appeared to be primarily dependent on the virus baseline growth dynamics. Further dose escalation studies are needed to examine the role of ART in the treatment of CMV infection in the transplantation setting.<sup>20</sup>

Despite the availability of effective antiviral therapy and reliable diagnostic assays, cytomegalovirus (CMV) has remained a significant complication after hematopoietic stem-cell transplantation (HSCT) [6].

All currently available anti-CMV drugs, including ganciclovir, foscarnet, and cidofovir, target the viral DNA polymerase. Their use is limited by toxicity, low oral bioavailability (with the exception of the oral prodrug valganciclovir), and drug resistance [6, 47]. These limitations, along with the epidemiological shift of CMV infection, requiring repeated and prolonged treatment courses, create an increasing need for new, effective, and better-tolerated antiviral drugs.

The benzimidazole l-ribose maribavir which targets the UL97 kinase has held promise as an alternative treatment for CMV infection [89]. However, recent results from a phase III study have not revealed a significant impact on the rate of CMV disease following HSCT.

---

<sup>20</sup> This work was supported by grants from the Israeli Ministry of Health and the Israel Science Foundation (D.G.W), the HHV-6 Foundation (M.M.), the Bayerische Forschungsförderung (M.M., T.S.), and NIH grant AI39938 (S.C). Artesunate tablets were generously provided by Dafra Pharma, Belgium.

Recently, the anti-malaria drug ART has been shown to be an effective inhibitor of human CMV *in vitro* and in an experimental animal model [21, 22, 35, 71]. Importantly, the extensive use of artesunate in malaria patients has not been associated with significant adverse effects [22]. These characteristics raise the possibility that ART could represent a safe therapeutic option for CMV infection in immunocompromised patients.

We have recently described the successful clinical use of ART for the treatment of CMV in a single patient who developed drug-resistant infection during preemptive antiviral therapy after HSCT [73].

## 5.2 Results

Here we report the first case-series of 6 HSCT recipients who received preemptive artesunate treatment for CMV infection; utilizing frequent viral load monitoring, we have examined the viral kinetics following institution of ART, and further employed first-phase viral kinetics studies to determine its antiviral effectiveness.

Of the 6 patients, one (Table 4, Patient #1) received preemptive artesunate treatment on a compassionate basis due to increasing viral load with emergence of multi-drug-resistant L776M DNA polymerase (*pol*) mutant [73]. Five patients (Table 4, patients #2–6) were enrolled in a pilot study aimed to evaluate the safety and efficacy of artesunate in preemptive treatment of CMV infection in HSCT recipients >18 years, who had detectable CMV DNA with >2000 DNA copies/ml. Eligible patients in this study received preemptive treatment with oral artesunate (Dafra Pharma, Belgium; 200 mg × 2/day for one day,

followed by 100 mg × 1/day for 28 days). CMV DNA load was determined on days 0, 3, 7, 14, 21, 28 of treatment by real-time PCR assay as described [5]. Artesunate was discontinued upon lack of clear virological response (defined as viral load increase or decrease by <0.5 log DNA copies/ml) on days 7, 14 and 21. These strict criteria were employed to prevent deterioration during treatment. (For more details of the study design, see ClinicalTrials.gov NCT00284687; The study was approved by the Institutional and National Ethics Committees and performed according to the Declaration of Helsinki, Good Clinical Practice guidelines, and the Human-Experimentation Guidelines of the Israeli Ministry of Health. All participants gave written informed consent).

Pt #	Gender/age, y	Underlying disease	Type of HSCT	Time of viremia post HSCT, days	Baseline Viral load, (copies/ml)/DT (days)/S <sub>0</sub>	viral load kinetics at 7 days of artesunate treatment	Calculated antiviral effectiveness (%) <sup>a</sup>	Artesunate treatment outcome (ε)	Clinical & virological outcome following treatment <sup>b</sup>
1 <sup>c</sup>	M/12	X-linked adrenoleukodystrophy	Haploidentical T-cell-depleted	147; 357	1.15 × 10 <sup>6</sup> ; 32,500/7.6	1.7–2.1 log decline; T <sub>1/2</sub> 0.9–1.9 days; D 0.98	90	Completed 56 days (2 treatment courses)	Asymptomatic; no rebound viremia for 76d
2	F/66	Diffuse large B cell lymphoma	Autologous	28	2,500/1.8	0.8 log decline; T <sub>1/2</sub> 1.8 days; D 0.75	82	Completed 28 days	Asymptomatic; no rebound viremia for 1 y
3	M/42	Acute lymphocytic leukemia	Mismatched	90	50,000/1.4/0.56	Stabilization; S <sub>A</sub> 0.25	57	Discontinued at 7 days	CMV disease; Continued deterioration with foscarnet
4	M/65	Acute myelocytic leukemia	Matched unrelated	81	24,000/1.8/0.39	Stabilization; S <sub>A</sub> 0.06	84	Discontinued at 7 days	Asymptomatic; Rapid response to ganciclovir
5	M/46	Acute myelocytic leukemia	haploidentical non-T-cell-depleted	35	12,400/0.98/0.71	0.86 log increase; S <sub>A</sub> 0.28	60	discontinued at 7 days	Asymptomatic; Rapid response to ganciclovir
6	F/52	Acute myelocytic leukemia	Matched unrelated	34	12,000/1.3/0.52	0.65 log increase; S <sub>A</sub> 0.30	43	Discontinued at 7 days	Asymptomatic; Rapid response to ganciclovir

Table 4: Demographic, clinical, and virological characteristics of HSCT recipients receiving preemptive artesunate treatment

DT indicates doubling time; S<sub>0</sub> and S<sub>A</sub> represent the exponential viral growth slopes before and immediately after the initiation of ART treatment (relevant

for patients #3–6).;  $T_{1/2}$  indicates viral decay half life; D represents the magnitude of the first-phase viral decline in log10 base (relevant for patients #1,2)

a Calculated as indicated in “Patients and Methods” section: for patients #1,2,  $\varepsilon = 1 - 10^{-D}$ , for patients #3–6,  $\varepsilon = 1 - S_A/S_0$

b Following completion or discontinuation of artesunate treatment.

c Patient 1 had received 2 courses of preemptive ART on a compassionate basis as previously reported.

The viral doubling time and decay half life ( $T_{1/2}$ ) were calculated on the basis of the best-fit curve by use of the equation  $(\ln 2)/a$ , where “ $a$ ” is the logarithmic slope [24]. The antiviral effectiveness of artesunate ( $\varepsilon$ ) was calculated in two ways: For patients with an early decline in viremia, we used the magnitude of the first-phase viral decline (D in log10 base) in the equation  $\varepsilon = 1 - 10^{-D}$  [56]. For patients with delayed virological response we used the equation  $\varepsilon = 1 - S_A/S_0$  where “ $S_A$ ” and “ $S_0$ ” represent the exponential viral growth slopes immediately after and before the initiation of treatment, respectively, according to the model developed by Neumann *et al.* for viral kinetics [56].

Two patients (patients #1 and #2; Table 4 and Figure 23) successfully completed 28 days of ART treatment. These patients exhibited a rapid decline in viral load, with 0.8–2.1 log decline by 7 days of treatment and a viral  $T_{1/2}$  of 0.9–1.9 days (see Table 1). These viral decay kinetics are consistent with those previously reported for ganciclovir and foscarnet [24]. Based on the first-phase viral decline, a high antiviral effectiveness (82–90%) was calculated.

In the four remaining patients (patients #3–6), ART was discontinued at 7 days of treatment, in accordance with the study criteria, due to the development of CMV disease (patient #3) or lack of clear virological response (patients #4–6). While no viral load decline was observed in these patients by 7 days of ART treatment, all four demonstrated a stalled viral growth slope during treatment ( $S_A$ ) when compared to baseline growth rate ( $S_0$ ) (see Table 4, Figure 23). These viral dynamics revealed some, albeit variable and limited antiviral effectiveness, ranging from 43% to 84% in patients #3–6 (Table 4). Notably, three of these patients (patients #4–6) rapidly responded to ganciclovir [24], with a 1.4–1.8 log decline at day 7 of ganciclovir treatment – suggesting a lower antiviral efficacy of ART, in its current dosing regimen, when compared to ganciclovir.

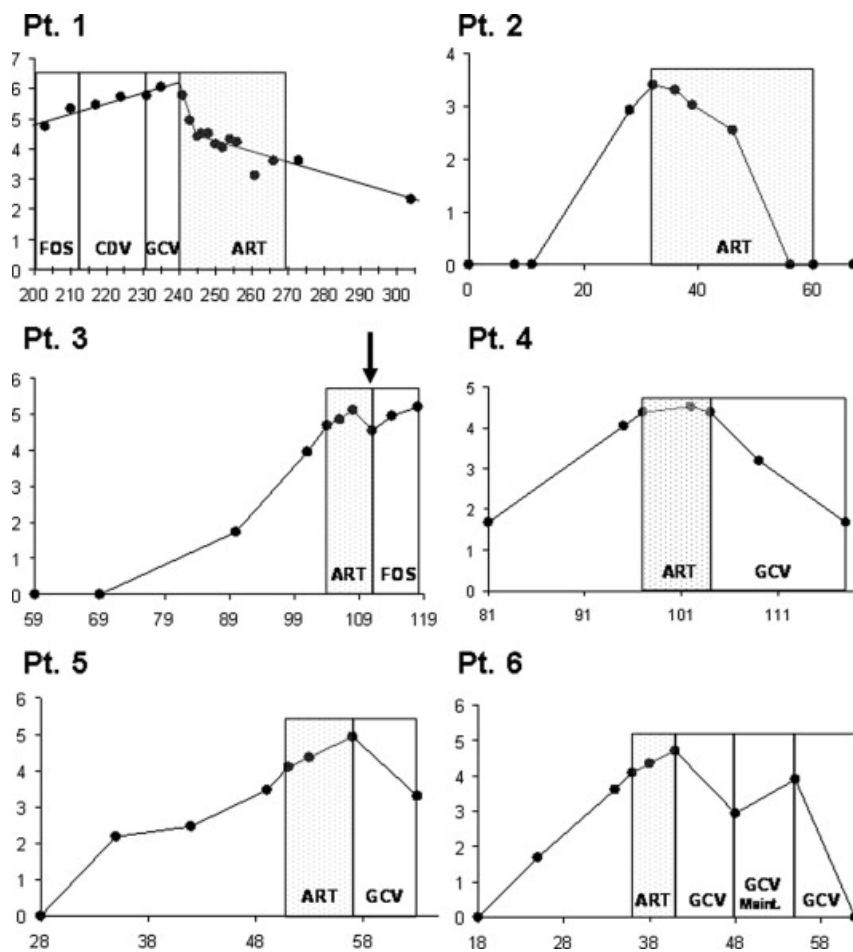


Fig. 23: CMV DNA load kinetics and antiviral treatment in HSCT recipients receiving preemptive artesunate treatment. Y axis values, log DNA copies/ml; X axis values, days after HSCT; arrow, time of disease development; ART, artesunate; GCV, ganciclovir; CDV, cidofovir; FOS, foscarnet; Maint., maintenance treatment.

However, it is important to interpret these findings with caution, as an initial lag phase of virologic response has been also reported in high-risk patients receiving ganciclovir [10, 59]. Thus, the small number of patients, and the early discontinuation of *artesunate* in 4 of the 6 patients preclude conclusions regarding its relative antiviral efficacy in heavily immunosuppressed patients.

### 5.3 Discussion

We sought to elucidate the basis for the enhanced response to artesunate in patients #1 and #2 when compared to patients #3–6; The rapid viral load decrease in patient #2 could be attributed to an earlier reconstitution of the host immune response following autologous HSCT, along with a low baseline viral load (Table 4), a well-known predictor of viral eradication. Yet, these factors could not account for the effective block of viral replication by artesunate in patient #1, who had received a T-cell depleted haploidentical HSCT, and exhibited a high baseline viral load of  $>10^6$  copies/ml. Limited analysis of artesunate and dihydroartemisinin concentrations in available plasma samples by the liquid chromatography–mass spectrometry method [88], did not show significant differences between the patients (data not shown), and thus could not explain the different response rates. Importantly, patient #1 harbored a mutant virus containing a *pol* L776M substitution, previously shown to confer a slight

replication defect in cell culture [73]. Furthermore, analysis of the mutant-virus baseline growth kinetics revealed a slow *in vivo* growth rate, with a prolonged doubling time of 7.6 days (Table 4). Thus, the attenuated growth of the mutant could have accounted for the enhanced response to ART in this case.

To further examine if the L776M *pol* mutation confirmed increased artesunate susceptibility, we compared the artesunate IC<sub>50</sub> of a recombinant mutant strain, containing the L776M mutation and a wild type control virus, using a secreted alkaline phosphatase (SEAP) activity assay as described [72, 73]. The artesunate IC<sub>50</sub> of the mutant ( $1.68 \pm 0.30 \mu\text{M}$ ) was slightly lower than that of the wild type ( $2.53 \pm 0.96 \mu\text{M}$ ), as revealed in 14 replicate assays spread over 4 setup dates. Further testing with artemisinin demonstrated similar trend for increased susceptibility of the mutant (IC<sub>50</sub>  $14.6 \pm 4.1 \mu\text{M}$  versus  $35.3 \pm 11.1 \mu\text{M}$ , in 4–7 replicates over 2 setup dates). These findings may be relevant towards the future use of artesunate in patients with drug-resistant CMV mutants, especially those demonstrating reduced fitness. Experiments are currently underway to examine its activity against various drug-sensitive and drug-resistant clinical isolates.

In view of the limited and diverse response to artesunate as demonstrated herein, a prophylactic rather than preemptive treatment study design, and a dose escalation study with close pharmacokinetic monitoring should be considered in future trials. The safety of this approach is supported by the low rate of toxicity reported for artesunate [22, 35], and the lack of adverse events in the 6 HSCT recipients treated over 7–56 days. We believe that the favorable safety profile of artesunate, along with its unique mechanism of antiviral activity,

involving inhibition of early replication steps [21, 22, 35] will make it an attractive candidate for combination antiviral drug therapy. In this regard, artesunate has been shown to exert an additive in vitro antiviral effect when combined with any of the currently available anti-CMV drugs [22, 35]. Combined ganciclovir-artesunate treatment could potentially allow for reduced dosage of ganciclovir and thus limit its bone marrow toxicity.

#### **5.4 Conclusions**

In conclusion, these first-phase viral kinetics studies in 6 HSCT recipients who received preemptive artesunate treatment revealed a divergent antiviral efficacy of artesunate, ranging from 43% to 90%, which appeared to be primarily dependent on the virus baseline growth dynamics. Further dose escalation studies are needed to examine the role of artesunate in the treatment of CMV infection in the transplantation setting.

## **Chapter 6**

### **Discussion and conclusions**

#### **6.1 Methodological considerations**

This multifaceted work has propelled our understanding of HBV and CMV viral kinetics and has also brought something valuable to the systems biology/modeling world. In the first two projects, we introduced two novel mathematical models. The HBV model is a cellular model and incorporates the HBeAg as a variable as well as the effects of immune response modeled as functional effects on the viral dynamics. From our unique data set, we learned more about the relationship between viral decline and the role of HBeAg. It appears that HBeAg negativity is irrespective of viral decline and thus depends on some other mechanism. We hypothesized that HBeAg was linked to the number of infected cells and therefore could be used as a surrogate marker of

the number of infected cells remaining in the system following and during treatment with an antiviral drug. For HBV we did not include intracellular dynamics into the model. This will be for future works.

For CMV, on the other hand, we introduced a novel 7-dimensional mathematical model that includes intracellular replication dynamics. This appropriately describes the HM profile (and the other patterns observed) and supports our hypothesis that an intracellular feedback loop between UL97 and GCV is the underlying biological reason for the frequently observed HM profile pattern. Since whole blood samples involve cell-associated virus, this has important indications for mathematical modeling since intracellular processes leading to the production of cell-associated and plasma virus may be altered due to antiviral treatment and/or the level of immunosuppression. We propose that intracellular models are the future to further our understanding of antiviral drug therapy in general and the likely decay patterns that are associated with current drugs that rely upon viral kinases for activation and for new drugs in development.

The third work involved estimation of viral decay rates using a linear best-fit curve model and revealed that the antiviral efficacy of *Artesunate* was mostly dependent on the viral load at baseline. This work was limited by the number of patients and low frequency of sampling, thus more elaborate and detailed modeling was not possible.

In general, our analysis shows that it is not appropriate to consider all patients undergoing treatment with GCV for CMV infection as belonging to the same

kinetic profile pattern, as has been done in previous studies. In so doing, we identified a hump profile as a frequent kinetic pattern that has not been reported before. Our data show that the early control of viral replication (1<sup>st</sup> phase) is indicative of how effective viral control will be in the 2<sup>nd</sup> phase regardless of whether this phase is early or late and also regardless of whether the slope was increasing or flat and provides a rationale for early assessment in CMV loads in the evaluation of new drugs for CMV.

## **6.2 HBV**

Our endeavor to understand the relationship between HBeAg status and HBV viral load decay lead us to many interesting observations. Most importantly, we were able to validate our novel model by comparing viral load and HBeAg data with viral load and HBeAg decay kinetic patterns in the context of placebo and treatment. We found that HBeAg loss can occur in the context of PLB and also in the context of treatment. Presumably, the PLB scenario implies that HBeAg loss is induced by an active, competent immune response component and we were able to model this by using/modifying an immune response parameter representative of this competency. We also found that HBeAg loss can occur in the context of antiviral treatment and that this loss was not dependent on the dose of treatment. This was also confirmed by the model. This is an interesting finding as in the clinical setting, it may not be necessary to use a higher dose (30 mg) of Adefovir. We also found that when HBeAg occurs as a result of treatment as opposed to placebo, the viral load is significantly lower at the time

this occurs. However, the time that it takes to HBeAg loss is approximately the same as for placebo.

Using the model, we also were able to confirm that patients could remain HBeAg positive in spite of decline of viral load to undetectable levels by altering the loss rate parameter for HBeAg. This implies that it may be advisable for patients who remain HBeAg positive to undergo immune enhancement therapy in tandem with antiviral treatment [69]. If in fact HBeAg is closely linked to the number of cccDNA-infected cells, which we have provided evidence for, then it seems clear that efforts to lower the number of infected cells by direct immune enhancement at the time of treatment initiation would be an effective way to reduce the number of infected cells and subsequently induce HBeAg loss in these patients to promote a better clinical prognosis. We confirmed this with the model and in fact, we saw a transition from HBeAg positive status to negative when we increased the value of  $m$  at day 0.

Resurgence of the virus would be more likely in a patient who remained HBeAg positive even if their viral load declined to undetectable levels. This is because it would indicate that the number of cccDNA-infected cells is high as well. Subsequently, in these patients, continued treatment may be the right course of action and as previously mentioned, immune enhancement may be a prudent course of action.

We independently examined the effects of antivirals and the immune response on the virus load and HBeAg loss and were able to develop an analytical expression to predict the viral load at the time that HBeAg becomes

undetectable ( $V_{Neg}$  and  $t_{Neg}$ , respectively). We found that both antivirals and the immune response could cause HBeAg loss but that  $V_{Neg}$  was independent of the immune response. However, we found that  $t_{Neg}$  is highly dependent on the effectiveness of the immune response. These findings correspond to data providing evidence to support the claim that HBeAg decline is indicative of the number of persistent ccc-DNA-infected cells and thus shows promise as an effective predictive tool.

In response to the question of whether or not HBeAg can be used as a surrogate marker of the number of infected cells, we propose an extension of the current novel model of HBV infection. We propose this due to the fact that our model does not take into account the number of cccDNAs per cell. As previously mentioned, long-term ADV therapy significantly decreases cccDNA levels by a primarily noncytolytic mechanism [86] which is linked to HBeAg<sup>-</sup> status [30]. Thus, future work may involve extending our current model of HBV infection model to include an intracellular component to account for this or possibly other factors. If we imagine a situation where an individual has a high number of cccDNA-infected cells but with few cccDNAs per cell, then the decay kinetics might differ from an individual with a high number of cccDNA-infected cells with many cccDNAs per cell. This will also depend on the individual's response to treatment, their immune response competency and other factors. A model that incorporates this concept might be a better tool to work with as we would then be able to theoretically use HBeAg as a surrogate marker for the number of cccDNAs per cell rather than for the absolute number of infected cells. A complication with doing this is that total cccDNAs per cell are

measured from a biopsy site and does not account for a bird's-eye-view of the system.

Ultimately, it seems as though it would be prudent to introduce an immune enhancement regimen in tandem with a lower dose of adefovir in order to promote HBeAg loss and seroconversion to anti-HBe. This would in fact reduce the viral load, the number of cccDNA-infected cells and perhaps promote antibody production.

HBsAg is another copious antigen produced as a by-product of HBV replication. HBsAg concentration decline is very slow during treatment (HBsAg loss is also observed in only a small fraction of patients) leading to the current hypothesis that HBsAg has a very long half-life which aids in the persistence of the virus. Again, recent evidence based on analysis of HBsAg kinetics measured with quantitative assays has led us to hypothesize that this paradigm is wrong and in fact HBsAg declines slowly because of continuous production during treatment. This would be another topic of investigation for future research and would also be interesting to model. For example, if we expanded the model to include another variable to represent HBsAg then hypothetically we could make predictions pertaining to HBsAg levels and test the findings against observations from data. Open questions may include whether or not all infected cells containing cccDNA produce HBsAg and also the relationship between HBsAg decline and cccDNA loss and viral load decay.

More recently, VIREAD (*tenofovir disoproxil fumarate*) is a more potent drug used to treat chronic hepatitis B virus (HBV) in adults and is used to block the enzyme reverse transcriptase. It has also been used as part of multidrug

treatment to treat HIV and had been found to successfully treat HBV in some patients and has actually been found to be even more effective than Adefovir in some cases. A recent clinical trial testing the efficacy of Tenofovir in reducing viral load and antigen load showed about 90% of patients become HBV-DNA undetectable but the rates of HBeAg and HBsAg loss (20% and 5%) do not increase much compared to Adefovir [93]. It would be interesting to apply our model to kinetic data for Tenofovir as it may prove useful in validating our model and also may provide new insights into the discrepancy between HBeAg loss and viral load decline for a new set of patients.

### **6.3 CMV**

The CMV model is a novel intracellular model that incorporates and introduces the concept that a negative feedback loop exists between the anti-CMV drug *Ganciclovir* and a replication by-product of the virus itself, UL97. This feedback loop results in differential kinetic profile patterns and allowed us for the first time to explain why during GCV therapy of CMV we see viral kinetic patterns not previously observed or reported.

Our analysis shows that it is not appropriate to consider all patients undergoing treatment with GCV for CMV infection as belonging to the same kinetic profile pattern, as has been done in previous studies. In so doing, we identified a hump profile as a frequent kinetic pattern. Our data show that the early control of viral replication is indicative of how effective viral control will be in the 2<sup>nd</sup> phase making early assessment vital. Of utmost relevance in the clinical setting, early changes in viral kinetic patterns can be used to predict the treatment regimen according to dose and duration. For example, if within the first 7-21 days a

patient is exhibiting an HM profile, then it would be tolerable to withdraw treatment at day 21 due to drug toxicity since the viral load continues to decline post day 21 according to mathematical projections. Also, we predict that patients with an RB profile may be slow HMs. This means that treatment should be continued post day 21 and can be done so at a lower dose.

Importantly, GCV is not the only anti-herpes drug currently in use that requires its target virus for metabolism. Acyclovir, a very commonly prescribed anti-herpes drug [79], also requires hCMV UL97 for phosphorylation. It would be very interesting to comb existing data sets for Acyclovir to see if these kinetic profile patterns exist there. If we found them there, it would add great merit to our theory. Our findings could potentially be extended to include many other anti-herpes drugs as well such as Cyclopropavir and Valacyclovir.

Differences in intracellular parameters in our novel 7-dimensional model determine the kinetic profile patterns. This provides strong evidence to support our theory that differences in intracellular rates associated with the intracellular feedback loop between GCV and UL97 determine whether or not an individual will have an HM, BP, DL or RB profile. This is important to know especially in the context of an RB since our results indicate that the RB profile is nothing more than a slow HM profile. In fact, there was no correlation between resistance mutations (extensively documented in the VICTOR study) and RB patients. Our kinetic profile pattern distribution has allowed us to refute the hypothesis that RBs manifest this profile due to resistance. Furthermore, as long as individuals with this profile resume treatment, even at a lower dose, they will eventually experience undetectable viral load levels within a predicted 90 days.

If our predictions are correct, clinicians may get the ‘false’ impression within the first 21 days of treatment that patients manifesting the RB profile are not responding to treatment due to resistance issues when in fact they are, just slowly. This indicates that patients manifesting the RB profile in first 21 days of treatment should NOT discontinue treatment at day 21 in spite of (transient) rising viral load.

The fact that viral load transiently rises in individuals with the HM profile is ultimately not prognostically detrimental according to our findings. This may be a cautionary tale however. Years ago, we assumed that during the chronic phase of HIV infection the virus was ‘sleeping’ and that there were no detrimental effects occurring with respect to immunopathogenesis. It wasn’t until we used mathematical modeling to illuminate what was really going on that we found out that the virus was in fact replicating at very rapid rates and systematically destroying the immune system. In our case, we have not gone into detail as to the specific effects of the transient rise in viral load, but this would be an interesting point to explore in the future. For example, we did not explore the dynamics between wild-type and mutant strains of CMV. We do know that the individuals who manifested the HM profile did not have any drug-resistant mutations. However, it might be an interesting pursuit to incorporate an extra equation into the model to account for a mutant viral strain.

#### **6.4 Future direction for HBV and CMV works**

Our preliminary results from analyses of novel data-driven mathematical models for both HBV and CMV infection have provided us with a clearer picture of the appropriateness of current mathematical models in describing

viral and antigen kinetics on one hand and unique kinetic profile patterns on the other. Our HBV work has not only brought us a little closer to understanding the relationship between viral load decay, cccDNA infected cell loss and HBeAg status but has prompted further investigations. In addition to our idea of developing an intracellular model that incorporates the number of cccDNAs/cell, we have started to develop a new model based on the one described in this work. This new model incorporates two new variables that account for the HBeAb population and for the population of antigen: antibody complexes that inevitably form *in vivo* and presumably may account for discrepancies between HBeAg and HBeAb levels. That is, depending on the complexing rate or the amount of antigen antibody complexing, the levels of both would vary from patient to patient.

Another idea spurred from this work involves the concept a latent cell pool of HBeAg-producing infected cells. We have not started to develop this but it would be interesting in future works to investigate this further and to construct a model that includes a latent cell population producing HBeAg. It may be possible that resurgence of virus from newly activated latently-infected cells results in the subsequent maintenance of high levels of HBeAg.

Our CMV work has proved exciting on two fronts: with respect to modeling, we have brought a new model based on a completely new idea into circulation and used it to confirm our theory as to why we see different and new kinetic profile patterns in data. With respect to biology, we have used the model to show that the interaction between GCV and UL97 has a particular kinetic/clinical effect. This has vital clinical, pharmaceutical and general

scientific implications as the link between the unique viral kinetics and mode-of-action of GCV has never been reported.

Other future work could also include investigations involving pre-existing immunity as might be the case in DL patients, for example. Also, the effects that T-cell function has on viral kinetics would be a point of interest. CMV specific T cells are vital players in the fight to eradicate CMV from circulation therefore it might be prudent for us or other CMV modelers to incorporate a variable to represent this population. As previously mentioned, Grace Kepler has developed models of CMV infection to include the CD8 population as model variable so perhaps in the future we can combine our efforts.

## **6.5 Comparison of different viruses**

Ultimately, this multifaceted work has brought something valuable to the systems biology/modeling world. We had originally set out to do a comparative analysis of the viruses studied in this work with other viruses such as HIV and HCV but as with many scientific pursuits, this was not the final outcome. We found unique characteristics for the dynamical interactions of HBV and CMV with the drugs used to treat them that are significantly different than those for HIV and HCV. Thus one of the most important conclusions of this thesis is that it is vital to develop mathematical models that are specific for each virus/drug interaction rather than generic viral dynamics models.

## Bibliography

1. Ahmed E. and H.A. El-Saka (2010). *On fractional order models for Hepatitis C*. Nonlinear Biomed Phys. Mar 18; 4(1):1.
2. Anderson R.M. and R.M. May (1992). *Infectious diseases of humans: dynamics and control*, Oxford science publications, ISBN-10: 019854040X.
3. Asberg A., A. Humar, H. Rollag, A.G. Jardine, H. Mouas, M.D. Pescovitz, D. Sgarabotto, M. Tuncer, I.L. Noronha, A. Hartmann (2007). *Oral Gancyclovir is Noninferior to Intravenous Ganciclovir for the Treatment of Cytomegalovirus Disease in Solid Organ Transplant Recipients*, Am J Tranplant; 7: 2106-2113.
4. Avery R.K. (2007). *Valganciclovir Versus IV Ganciclovir for Therapy of Cytomegalovirus Viremia: Has Victory Been Achieved?* Am J Transplant; 7(9): 2062-2063.
5. Boeckh M., M. Huang, J. Ferrenber, T. Stevens-Ayers, L. Stensland, W.G. Nichols, L. Corey (2004). *Optimization of quantitative detection of cytomegalovirus DNA in plasma by real-time PCR*, J. Clin. Microbiology, 42 (3), pp. 1142–1148.
6. Boeckh M. and P. Ljungman (2009). *How we treat cytomegalovirus in hematopoietic cell transplant recipients*, Blood, 113 (23), pp. 5711–5719.

7. Boyce W.E. and DiPrima R.C., *WIE Elementary Differential Equations and Boundary Value Problems*, 8th Edition, John Wiley and Sons, Inc., 2006.
8. Brunetto M.R. *et al.* (2004). *Treatment of HBeAg-Negative Chronic Hepatitis B with Conventional or Pegylated Interferon*, Manuscript from the presentations at the International Conference on the Management of Patients with Viral Hepatitis, Paris.
9. Brunetto M.R. and A.S. Lok (2010) *New approaches to optimize treatment responses in chronic hepatitis B*. *Antiviral Therapy*; 15 Suppl. 3:61-8.
10. Buyck H.C., P.D. Griffiths and V.C. Emery (2010). *Human cytomegalovirus (HCMV) replication kinetics in stem cell transplant recipients following anti-HCMV therapy*, *J. Clin. Virol.*, 49 (1), pp. 32–36.
11. Cantisán Bohórquez S. and Navarro D. Ortega (2011). *Immunological monitoring strategies for cytomegalovirus infection*. Immune-based therapies, *Enferm Infecc Microbiol Clin*. Dec; 29 Suppl 6:28-32.
12. Carman W.F., M.R. Jacyna, S. Hadziyannis, P. Karaviannis, M.J. McGarvey, A. Makris, H.C. Thomas (1989). *Mutation preventing formation of hepatitis B e antigen in patients with chronic hepatitis B infection*. *Lancet*; 2: 588-591.
13. Chamberlain N.R. (2009). *The Big Picture Medical Microbiology: Lymphoreticular and Hematopoietic Infections*, pp.199-209, McGraw Hill, New York, NY.
14. Chan H.L., N.W. Leung, M. Hussain, M.L. Wong, A.S. Lok (2000). *Hepatitis B e antigen negative chronic hepatitis B in Hong Kong*. *Hepatology*, 3: 763-768.

15. Cirocco R.E., G. Ciancio, V. Esquenazi, G.W. Burke, J. Miller (1999). *Post Kidney Transplant CMV Incidence in the Gancyclovir Era: Monitoring Viral DNA by a CMV PCR Assay*. *Transplant Proc.* Feb-March; 31(1-2):1362-3.
16. Colombatto P. *et al.* (2004). *A new bio-mathematical model to describe the dynamics of HBV-DNA and infected hepatocytes in HBeAg negative/anti-HBe positive chronic hepatitis B patients treated with peginterferon alpha 2a (40KD) (Pegasys), lamivudine, or Pegasys plus lamivudine combination*. *J Hepatology*; 40:S125.
17. Colombatto P. *et al.* (2006). *A multiphase model of the dynamics of HBV infection in HBeAg-negative patients during pegylated interferon- $\alpha$ 2a, lamivudine and combination therapy*, *Antiviral therapy*, vol. 11, n<sup>o</sup>2, pp. 197-212.
18. Cooksley H., S. Chokski, Y. Maayan, H. Wedemeyer, P. Andreone, R. Gilson, T. Warnes, S. Paganin, F. Zoulim, D. Frederick, A.U. Neumann, C.L. Brosgart, N.V. Naoumov (2008). *Hepatitis B virus e antigen loss during adefovir dipivoxil therapy is associated with enhanced virus-specific CD4+ T-cell reactivity*. *Antimicrob Agents Chemother.* Jan; 52(1):312-20.
19. Cooksley W.G., T. Piratvisuth, S.D. Lee, V. Mahachai, Y.C. Chao, T. Tanwandee *et al.* (2003) *Peginterferon alpha-2a (40 kDa): an advance in the treatment of hepatitis B e antigen-positive chronic hepatitis B*. *J Viral Hepat*; 10:298-305.
20. Edelstein-Keshet L. (2005). *Mathematical Models in Biology*. Random House, New York.

21. Efferth Y., M. Marschall, X. Wang, S.M. Huong, I. Hauber, A. Olbrich, M. Kronschnabl, T. Stamminger, E.S. Huang (2002). *Antiviral activity of artesunate towards wild-type, recombinant, and ganciclovir-resistant human cytomegaloviruses*, J. Mol. Med., 80 (4), pp. 233–242.
22. Efferth T., M.R. Romero, D.G. Wolf, T. Stamminger, J.J. Marin, M. Marschall (2008). *The antiviral activities of artemisinin and artesunate*, Clin. Infect. Dis., 47 (6), pp. 804–811.
23. Emery V.C., A.V. Cope, E.F. Bowen, D. Gor, P.D. Griffiths (1999). *The dynamics of human cytomegalovirus replication in vivo*, J. Exp. Med., 190 (2), pp. 177–182.
24. Emery V.C. and P. Griffiths (2000). *Prediction of cytomegalovirus load and resistance patterns after antiviral chemotherapy*. PNAS July 5, vol. 97 no. 14 8039-8044.
25. Emery V.C. (2011). *Could a vaccine against immune-evading cytomegalovirus become a reality?* Expert Rev Vaccines. Aug; 10(8):1109-11.
26. Emery V.C., K. Asher and Cde J. Sanjuan (2012). *Importance of the cytomegalovirus seropositive recipient as a contributor to disease burden after solid organ transplantation*, J Clin Virol. June; 54(2):125-9.
27. *Fundamental Virology*, 2<sup>nd</sup> Edition, Raven Press, New York, 1991.
28. Fried, M.W. et al. (2008). *HBeAg and hepatitis B virus DNA as outcome predictors during therapy with peginterferon alfa-2a for HBeAg-positive chronic hepatitis B*, Hepatology, Volume 47 Issue 2, Pages 428-434.
29. Ganem D. and A.M. Prince (2004). *Hepatitis B virus infection - natural history and clinical consequences*. N. Engl. J. Med. 350, 1118-1129.

30. Guner R, M. Karahocagil, M. Buyukberber, O. Kandemir, O. Ural, G. Usluer, D. Inan, I. Koksal, N. Baykam, K. Hizel, T. Yamazhan, S. Esen, M.A. Tasyaran (2011). *Correlation between intrahepatic hepatitis B virus cccDNA levels and other activity markers in patients with HBeAg-negative chronic hepatitis B infection*. Eur J Gastroenterol Hepatol. Nov; 23(12):1185-91.
31. Ho D.D., A.U. Neumann, A.S. Perelson, W. Chen, J.M. Leonard, M. Markowitz (1995). *Rapid turnover of plasma virions and CD4 lymphocytes in HIV-1 infection*. Nature 373 123-26.
32. Hou J.L., H. Ma, J. Sun, Q. Xie, Y. Xie, Y.T. Sun, H. Wang, G.F. Shi, M.B. Wan, J.Q. Niu, Q. Ning, Y.Y. Yu, M. Jiang, *Baseline and early on-treatment characteristics in HBeAg-positive patients with chronic hepatitis B infection achieving an early on-treatment response to pegylated interferon alfa-2a (40KD): interim results from the RGT study*, 62th Annual Meeting of the American Association for the Study of Liver Diseases San Francisco 2011 Nov 6-9.
33. Humar A. *et al.* (2008) *An assessment of Herpesvirus Co-infections in Patients with CMV disease: a correlation with Clinical and Virological Outcomes*. Am. J. Transplant.
34. Janeway C.A. P. Travers, M. Walport, M. Schlomchik (2001). *Immunobiology*, Edition 5, Garland Publishing.
35. Kaptein S.J., T. Efferth, M. Leis, S. Rechter, S. Auerochs, M. Kalmer, C.A. Bruggeman, C. Vink, T. Stamminger, M. Marschall (2006). *The anti-malaria drug artesunate inhibits replication of cytomegalovirus in vitro and in vivo*, Antiviral Res., 69 (2), pp. 60–69.

36. Kepler G.M., H.T. Banks, M. Davidian, E.S. Rosenberg (2008). *A model for HCMV Infection in Immunosuppressed Patients*, Mathematical and Computer Modeling, doi:10.1016.
37. Kepler G. et al. (2009). *Dynamic model for within-subject HCMV infection*, Mathematical and Computer Modeling 49 (7-8), 1653-1663.
38. Kuntz E. and H.D. Kuntz (2002). *Hepatology: Principles and Practice*, Berlin: Springer Verlag, ISBN 3540 42161 0.
39. Laras A., J. Koskinas, E. Dimou, A. Kostamena, S.J. Hadziyannis (2006). *Intrahepatic levels and replicative activity of covalently closed circular hepatitis B virus DNA in chronically-infected patients*, Hepatology, Volume 44, Issue 3, pages 694–702.
40. Lau J.Y., T.L. Wright (1993). *Molecular virology and pathogenesis of hepatitis B. Lancet* 342, 1335-1340.
41. Lau P.K.H., M.L. Woods, S.K. Ratanjee, G.T. John (2011). *Artesunate is Ineffective in Controlling Valganciclovir-Resistant Cytomegalovirus Infection*, Clin Infect Dis. 52 (2): 279.
42. Layden JE, T.J. Layden, K.R. Reddy, R.S. Levy-Drummer, J. Poulakos, A.U. Neumann (2002). *1st phase viral kinetic parameters as predictors of treatment response and their influence on the second phase viral decline. J Viral Hepatitis* 9:340-345.
43. Lequan M., L. Weidong, S. Yongmei, Y. Kuang (2008). *A Mathematical Model of the Dynamics for anti-HBV Infection Treatment with Peginterferon Alfa-2a*, pp. 1433-1436.

44. Lewin S.R., R.M. Ribeiro, T. Walters, G.K. Lau, S. Bowden, S. Locarnini *et al.* (2001) *Analysis of hepatitis B viral load decline under potent therapy: complex decay profiles observed.* Hepatology; 34:1012-1020.
45. Locarnini S. (2004). *Molecular virology of hepatitis B virus.* Semin. Liver Dis. 24 Suppl 1: 3–10.
46. Lok A.S., J. Heathcote and J.H. Hoofnagle, (2001). *Management of hepatitis B: 2000 - summary of a workshop.* Gastroenterology; 120:1828-1853.
47. Lurain N.S., S. Chou, (2010). *Antiviral drug resistance of human cytomegalovirus,* Clin. Microbiol. Rev., 23 (4), pp. 689–712.
48. Malmström S., A. Eilard, S.B. Larsson, C. Hannoun, G. Norkrans, M. Lindh (2012). *Genotype impact on long-term virological outcome of chronic hepatitis B virus infection,* J Clin Virol. May 17.
49. Marcellin P., T.T. Chang, S.G. Lim, M.J. Tong, W. Sievert, M.L. Shiffman, L. Jeffers, Z. Goodman, M.S. Wulfsohn, S. Xiong, J. Fry, C.L. Brosgart (2003). *Adefovir dipivoxil for the treatment of hepatitis B e antigen-positive chronic hepatitis B.* N Engl J Med. Feb 27;348 (9):808-16.
50. Marcellin P., G.K. Lau, F. Bonino, P. Farci, S. Hadziyannis, R. Jin *et al.* (2004) *Peginterferon Alfa-2a HBeAg-Negative Chronic Hepatitis B Study Group. Peginterferon alfa-2a alone, lamivudine alone, and the two in combination in patients with HBeAg negative chronic hepatitis B,* New England J. Med; 351:1206-1217.
51. Mukherjee S. (2003). *Adefovir dipivoxil for hepatitis B e antigen-positive chronic hepatitis B.* N Engl J Med. Feb 27; 348 (9): 808-16.
52. Murray, J.M., Purcell R.H., S.F. Wieland (2006). *The half-life of hepatitis B virions,* Hepatology, 44, 1117-1121.

53. Murray J.M., Wieland S.F., Purcell R.H., F.V. Chisari (2005). *Dynamics of hepatitis B virus clearance in chimpanzees*, Proceedings of the National Academy of Sciences USA, 102, 17780-17785.
54. Murray P.R., K.S. Rosenthal and M.A. Pfaller (2009). *Medical Microbiology*, 6th Edition. pp. 645-648, Mosby Elsevier, Philadelphia, PA.
55. Murray K., S.A. Bruce, A. Hinnen, P. Wingfield, P.M. van Erd, A. de Reus, H. Schellekens (1984). *Hepatitis B virus antigens made in microbial cells immunise against viral infection*. EMBO J. March; 3(3): 645–650.
56. Neumann A.U., N.P. Lam, H. Dahari, D.R. Gretch, T.E. Wiley, T.J. Layden, A.S. Perelson (1998). *Hepatitis C viral dynamics in vivo and the antiviral efficacy of interferon-alpha therapy*, Science, 282 (5386), pp. 103–107.
57. Neumann A.U., Y. Havlin, T. Ronen, M. Tsiang, M. Wulfsohn, C. Brosgart et al. (2003). *Predicting HBeAg loss by HBV DNA early kinetics and HBV genotype during treatment of HBeAg<sup>+</sup> chronic hepatitis B patients with adefovir dipivoxil* [Abstract], J Hepatol; 38(Suppl 2):26.
58. Neumann A.U. (2005). *Hepatitis B viral kinetics – a dynamic puzzle still to be resolved* (Editorial), Hepatology, 42:249-254.
59. Nichols W.G., L. Corey, T. Gooley, W.L. Drew, R. Miner, M. Huang, C. Davis, M. Boeckh (2001). *Rising pp65 antigenemia during preemptive anticytomegalovirus therapy after allogeneic hematopoietic stem cell transplantation: risk factors, correlation with DNA load, and outcomes*, Blood, 97 (4) (2001), pp. 867–874.
60. Nowak M. and R. May (2000). *Virus Dynamics: Mathematical Principles of Immunology and Virology*, Oxford University Press.

61. Nowak M.A., S. Bonhoeffer, A.M. Hill, R. Boehme, H.C. Thomas, H. McDade (1996). *Viral dynamics in hepatitis B virus infection*, Proc. Natl. Acad. Sci. USA, Vol. 93, pp. 4398–4402.
62. Nowak M. and C.R.M. Bangham (1996). *Population dynamics of immune responses to persistent viruses*, Science, Vol. 272, pp. 74-79.
63. Ott J.J., G.A. Stevens, J. Groeger, S.T. Wiersma (2012) *Global epidemiology of hepatitis B virus infection: New estimates of age-specific HBsAg seroprevalence and endemicity*, Vaccine, Volume 30, Issue 12, 9 March, Pages 2212–2219.
64. Park S.G. and G. Jung (2001). *Hsp60 Interacts with the Molecular Chaperonin Human Hepatitis B Virus Polymerase*, J. Virol. 75(15): 6962-6968.
65. Perelson A.S., A.U. Neumann, M. Markowitz, J.M. Leonard, D.D. Ho (1996). *HIV-1 dynamics in vivo: virion clearance rate, infected cell life-span, and viral generation time*, Science, 271, 1582-1586.
66. Perelson A.S., (2002). *Modeling viral and immune system dynamics*. Nat. Rev. Immunol. 2 28-36.
67. Razonable R.R. and V.C. Emery (2004). *Management of CMV infection and disease in transplant patients*. 27-29 February. 11th Annual Meeting of the IHMF (International Herpes Management Forum). Herpes. Dec;11(3):77-86.
68. Ribeiro R.M., A. Lo and A.S. Perelson (2002). *Dynamics of hepatitis B virus infection*, Microbes and Infection, Volume 4, Issue 8, July, Pages 829-835.
69. Sarin S.K., A. Sood, M. Kumar, A. Arora , D. Amrapurkar, B.C. Sharma, A. Konar , Y. K. Chawla, R.K. Jain, V. Nanda, A. Kumar, S. Hissar, P.

- Lavate, D. Lahoti (2007). *Effect of Lowering HBV DNA Levels by Initial Antiviral Therapy Before Adding Immunomodulator on Treatment of Chronic Hepatitis B*, *The American Journal of Gastroenterology* 102, 96–104.
70. Sayed S.K. and M.A. Kobeisy (2012). *The relationship between core promoter mutation of hepatitis B virus, viral load and hepatitis B e antigen status in chronic hepatitis B patients*. *Cell Immunol.* Apr 3.
71. Schnepf N., J. Corvo, M.J. Pors, M.C. Mazon (2010). *Antiviral activity of ganciclovir and artesunate towards human cytomegalovirus in astrocytoma cells*, *Antiviral Res.*
72. Scott G.M., A. Weinberg, W.D. Rawlinson, S. Chou (2007). *Multidrug resistance conferred by novel DNA polymerase mutations in human cytomegalovirus isolates*, *Antimicrob. Agents Chemother.*, 51 (1), pp. 89–94.
73. Shapira M.Y., I.B. Resnick, S. Chou, A.U. Neumann, N.S. Lurain, T. Stamminger, O. Caplan, N. Saleh, T. Efferth, M. Marschall, D.G. Wolf (2008). *Artesunate as a potent antiviral agent in a patient with late drug-resistant cytomegalovirus infection after hematopoietic stem cell transplantation*, *Clin. Infect. Dis.*, 46 (9), pp. 1455–1457.
74. Sia I.G., J.A. Wilson, C.M. Groettum, M.J. Espy, T.F. Smith, C.V. Paya (2000) *Cytomegalovirus (CMV) DNA load predicts relapsing CMV infection after solid organ transplantation*. *J Infect Dis.*, Feb; 181 (2): 717-20.
75. C. Steininger (2007). *Novel Therapies for Cytomegalovirus Disease*, *Recent Patents on Anti-Infective Drug Discovery*, 2, 53-72.

76. Strippoli G.F., E.M. Hodson, C.J. Jones, J.C. Craig JC (2006). *Pre-emptive Treatment for Cytomegalovirus Viremia to Prevent Cytomegalovirus Disease in Solid Organ Transplant Recipients*, *Transplantation: Volume 81(2)27*: January, pp 139-145.
77. Summers, J. and W.S. Mason (1982). *Replication of the genome of a hepatitis B-like virus by reverse transcription of an RNA intermediate*, *Cell*, 29:403–415.
78. Takkenberg B, V. Terpstra V, H. Zaaijer, C. Weegink, M. Dijkgraaf, P. Jansen, M. Beld, H. Reesink (2011). *Intrahepatic response markers in chronic hepatitis B patients treated with peginterferon alpha-2a and adefovir*. *J. Gastroenterol Hepatol*. 2011 Oct; 26(10): pp 1527-35.
79. Talarico C.L., C. T.C. Burnette, W.H. Miller, S.L. Smith, M.G. Davis, S.C. Stanat, T.I. Ng, Z. He, D.M. Coen, B. Roizman, K.K. Biron (1999). *Acyclovir Is Phosphorylated by the Human Cytomegalovirus UL97 Protein*, *Antimicrob Agents Chemother*. 43(8): pp. 1941–1946.
80. Toyama T, H. Ishida, H. Ishibashi, H. Yatsuhashi, M. Nakamuta, M. Shimada, H. Ohta, T. Satoh, M. Kato, T. Hijioka, H. Takano, T. Komeda, M. Yagura, H. Mano, Y. Watanabe, M. Kobayashi, E. Mita (2012). *Long-term outcomes of add-on adefovir dipivoxil therapy to ongoing lamivudine in patients with lamivudine-resistant chronic hepatitis B*, *Hepatol Res*. Apr 19.
81. Tsiang M., J.F. Rooney, J.J. Toole, C.S. Gibbs (1999). *Biphasic clearance kinetics of hepatitis B virus from patients during adefovir dipivoxil therapy*, *Hepatology*, Volume 29 Issue 6, Pages 1863-1869.

82. Van Quekelberghe S.A., S.A. Soomro, J.A. Cordonnier, F.H. Jansen (2008). *Optimization of an LC-MS method for the determination of artesunate and dihydroartemisinin plasma levels using liquid-liquid extraction*, J. Anal. Toxicol., 32 (2), pp. 133–139.
83. Wang C.C., C.J. Liu, M.Y. Lai, J.H. Kao, D.S. Chen (2007). *Dynamics of hepatitis B e antigen index ratio correlate with treatment response in chronic hepatitis B patients*, Liver international; 27 (2) :235-9.
84. Watkins R.R., T.L. Lemonovich, R.R. Razonable (2012). *Immune response to CMV in solid organ transplant recipients: current concepts and future directions*, Expert Rev Clin Immunol. May; 8(4):383-93.
85. Weifan G. and H. Jianming (2007). *Formation of Hepatitis B Virus Covalently Closed Circular DNA: Removal of Genome-Linked Protein*, Journal of Virology, June, p. 6164-6174, Vol. 81, No. 12.
86. Werle-Lapostolle B., Bowden S., S. Locarnini (2004). *Persistence of cccDNA during the natural history of chronic hepatitis B and decline during adefovir dipivoxil therapy*. Gastroenterology, 126, 1750-1758.
87. Whalley S.A., Murray J.M., Brown D., Webster G.J.M., Emery V.C., Dusheiko G.M., A.S. Perelson (2001). *Kinetics of acute hepatitis B virus infection in humans*. The Journal of Experimental Medicine, 193, 847-853.
88. William M. (2004). *The infectious etiology of chronic diseases: chronic hepatitis B infections*. National academies press, PMID: 22379643.
89. Winston D.J., J.A. Young, V. Pullarkat, G.A. Papanicolaou, R. Vij, E. Vance, G.J. Alangaden, R.F. Chemaly, F. Petersen, N. Chao, J. Klein, K. Sprague, S.A. Villano, M. Boeckh (2008). *Maribavir prophylaxis for prevention of cytomegalovirus infection in allogeneic stem cell transplant*

- recipients: a multicenter, randomized, double-blind, placebo-controlled, dose-ranging study*, Blood, 111 (11), pp. 5403–5410.
90. Wolters L.M., B.E. Hansen, H.G. Niesters, R.A. de Man (2002). *Viral dynamics in chronic hepatitis B patients during lamivudine therapy*. Liver. Apr; 22(2):121-6.
91. Wolters L.M., B.E. Hansen, H.G. Niesters, D. DeHertogh, R.A. de Man (2002). *Viral dynamics during and after entecavir therapy in patients with chronic hepatitis B*, J Hepatol; 37:137-144
92. Wolters L.M., B.E. Hansen, H.G. Niesters, R.S. Levi-Drummer, A.U. Neumann, S.W. Schalm *et al.* (2002). *The influence of baseline characteristics on viral dynamic parameters in chronic hepatitis B patients treated with lamivudine*. J Hepatol; 37:253-258.
93. Woo G., Tomlinson G., Nishikawa Y., Kowgier M., Sherman M., Wong D.K., Pham B., Ungar W.J., Einarson T.R., Heathcote E.J., M. Krahn (2010). *Tenofovir and entecavir are the most effective antiviral agents for chronic hepatitis B: a systematic review and Bayesian meta-analyses*. Gastroenterology. Oct; 139(4): 1218-29. Epub, 2010 Jun 20.
94. Wood P., *Understanding Immunology*, Prentice-Hall, Pearson Education LTD, 2001.
95. World Health Organization: Data and Statistics.
96. Wright T.L., *Treatment of Hepatitis B: The State of the Art*, Clinical Care Options for Hepatitis, Northwestern University, p.155.
97. Yodfat, Y., W. Thomas London, P. Whitford, W. Yochanan (1892) *A seroepidemiological study of Hepatitis B in a rural area in Israel*, American Journal of Epidemiology, Vol. 116, Issue 3, pp. 456-462.

98. Yousfi N., K. Hattaf and A. Tridane (2011). *Modeling the adaptive immune response in HBV infection*. J Math Biol. Nov; 63(5):933-57.
99. Zeuzem S., R.A. de Man, P. Honkoop, W.K. Roth, S.W. Schalm, J.M. Schmidt (1997) *Dynamics of hepatitis B virus infection in vivo*. J Hepatol 1997; 27:431-436.